Momentum, vorticity and transport: Considerations in the design of a finite-volume dynamical core

Todd D. Ringler

Abstract This chapter provides an end-to-end discussion of issues related to issues in the design and construction of dynamical cores. The governing equations of motion are derived from basic principles cast in the Lagrangian frame of motion. The Reynolds Transport Theorem is derived so that these conservation statements can be recast in their weak, integral form in the Eulerian reference frame. Special attention is given to the relationship between the momentum equation and vorticity dynamics. The principles of conservation of circulation and vorticity are derived in the continuous system. It is demonstrated that the kinematic principles related to circulation and vorticity can be carried over exactly into the discrete system. The analysis is conducted in an idealized, two-dimensional setting that is meant to serve as a prototype system for the consideration of the full three-dimensional general circulation of the atmosphere and ocean.

1 Introduction

More than forty years after the first global models for the simulation of the fluid motion in the atmosphere and ocean appeared, research into the construction of atmosphere and ocean "dynamical cores" has never been more vibrant. The dynamical core refers to the fluid-dynamic core of an atmosphere or ocean general circulation model; the part of the model that evolves the distribution of mass, momentum and tracer constituents forward in time. The diversity of approaches that are being explored to simulate the evolution of mass, momentum and tracers in the atmosphere and ocean systems points to both the richness and complexity of the problem.

The motivation for this chapter is to present an "end-to-end" view in the design of numerical models used for the simulation of fluid motion in the atmosphere and

Todd Ringler
Theoretical Division, Los Alamos National Laboratory, Los Alamos, NM 87545,
e-mail: ringler@lanl.gov

ocean. The process starts with a rigorous construction and description of the underlying continuous system. The process ends with the specification of a numerical model that is suitable for its target application. Both the beginning and end are essentially applied math activities, with the former manipulating continuous equations and the latter manipulating discrete equations. In between these ends is the ”art” of constructing dynamical cores. If the process were as simple as discretizing a set of continuous equations, we would not see the vibrancy in dynamical core development that we see today. A host of subtle, yet profound, questions such as ”which form of a continuous equations should be the starting point for the discrete model?” fall squarely in the middle of the end-to-end design process. This chapter explores some of those questions in order to illuminate the intricacies of the decisions that have to be made in the design process.

The price-to-be-paid for this end-to-end view is scope. Many relevant aspects of the design process have been omitted in order to contain the discussion to an appropriate length. The discussion is focused primarily on one important component of a dynamical core: the prediction of momentum. This proves to be an important and rich topic for several reasons. First, since the velocity that is derived from momentum acts as the transport velocity for the mass and tracers fields, a robust simulation of velocity is a prerequisite for any viable dynamical core. Furthermore, as the velocity field responds to changes in the applied forces it must also satisfy certain kinematic conditions, such as conservation of vorticity. Satisfying the desire to accurately model $\mathbf{F} = m\mathbf{a}$ while also accommodating important kinematic constraints is a challenge for any numerical model. And finally, the majority of the nonlinearity in dynamical core simulations arises from the simulation of the evolving velocity field. In many ways, getting the evolution of momentum ”right” is the hardest part in the design and construction of a dynamical core.

The analysis presented below is conducted in a very simple, two-dimensional framework and is, in some ways, quite removed from the global three-dimensional motions that compose the atmosphere and ocean general circulations. As such, it is important to address the relevance of this chapter to the modeling of the more complicated three-dimensional systems. First and foremost, the analysis conducted here is a prerequisite for the construction of a robust three-dimensional model. In that, what follows below could be considered a set of necessary, but not sufficient, properties of robust three-dimensional models of atmosphere and ocean circulations. Since the general circulation of the atmosphere and ocean occurs primarily along a vertical stack of two-dimensional sheets, it is folly to suppose that a numerical methods that performs poorly in the solution of the two-dimensional system will perform acceptably in the solution of the three-dimensional system. Second, while the two-dimensional system might seem trivial in some respects, many numerical methods used in the modeling of geophysical fluid dynamics fall short when viewed from the perspective of vorticity dynamics. Vorticity dynamics largely represent the ”slow modes” of these system where relatively small truncation errors can accumulate and, eventually, completely corrupt the simulation. The struggle to control the form of truncation error with respect to vorticity dynamics is as important today as it was when Arakawa wrote the seminal paper on the topic in 1966 (Arakawa, 1997).

And finally, this chapter is meant as an introduction to the concept of designing numerical methods that respect the continuous system in some relevant aspects. For this goal, the very simple, two-dimensional framework is perfectly appropriate.

The omissions in the discussion are sometimes glaring. For example, the importance of accurately simulating transport phenomena in dynamical cores is largely omitted [check cross reference]. The notable exception is the detailed discussion on the relationship between fluid acceleration and absolute vorticity transport. The next glaring omission is the lack of discussion of potential vorticity and its relationship to the velocity field; the discussion is based on an analysis of the absolute vorticity field. While absolute vorticity is connected only to the velocity field, potential vorticity is connected to both the velocity field and to the mass field. The analysis below can (and has) been extended from absolute vorticity to potential vorticity (Ringler et al, 2010). The choice was made based on the belief that a firm grasp of the absolute vorticity dynamics is a prerequisite to understanding the potential vorticity dynamics. And finally, while the primary target geometry of dynamical core is the surface of the sphere, the *f-plane* approximation is made through out. All of the analysis carries over to the sphere, the simplification to the *f-plane* is for the sake of conciseness in presentation. And finally, while the focus is on the relationship between the evolution of velocity and its relationship to vorticity dynamics, we need to be sure to understand that the velocity equation is derived from $\mathbf{F} = m\,\mathbf{a}$ and that the system can not be closed without the knowledge of the density field and the constitutive equation relating density to pressure.

The discussion unfolds in the following manner. First, the relevant evolution equations are constructed from the Lagrangian perspective. These conservation statements are then transferred to an Eulerian reference frame through the use of the Reynolds Transport Theorem (RTT). Since a full discussion of RTT is rarely found in texts related to geophysical fluid dynamics, RTT is derived from first principles for completeness. Following the development of the evolution equations appropriate for an Eulerian reference frame, a qualitative analysis is conducted of the various ”flavors” of the momentum equation that can be used as the basis for a numerical solution. The discussion then moves into the setting of discrete numerics by asking the most basic question of ”How we begin the process of discetization?” And finally, a numerical model is developed that meets the criteria developed throughout the entire discussion. The numerical model is constructed in such a way that it can easily be implemented in development environments such as MATLAB.

2 Reference Frames and Conceptual Constructs

When we consider the climate of the atmosphere or ocean, we expend considerable effort on the phenomena of transport, such as the transport of fluid density from one region to another, or the transport of tracer substance from a source region to a sink region, or the transport of momentum from one area to another. In almost

all cases, the most natural setting to consider transport is the *Lagrangian* reference frame where we, as the observer, move with the fluid.

To start, let us define a volume of fluid, V, composed of a set of particles, $\mathbf{R}$, enclosed at all times by a surface, S. Each particle in the set of $\mathbf{R}$ is denoted by its vector position $\mathbf{X}(t) = X_1\mathbf{e}_1 + X_2\mathbf{e}_2 + X_3\mathbf{e}_3$. As indicated, $\mathbf{X}$ is only a function of time. Also, $\mathbf{e}_{1,2,3}$ is the set of orthogonal unit vectors spanning the $\mathbb{R}^3$ space. See Figure 1. The idea of constructing the volume as a set of particles is entirely a conceptual construct; the particles are simply the most basic "element" that is used to define all other features; lines, surfaces and volumes can be "built" from sets of particles. Each particle is accompanied by an arbitrarily long list of labels representing such things as the particle position ($\mathbf{X}$), density (ρ) and velocity ($\mathbf{u}$). The validity of such an approach is that the particles can be made arbitrarily small and, thus, approach the continuum limit.

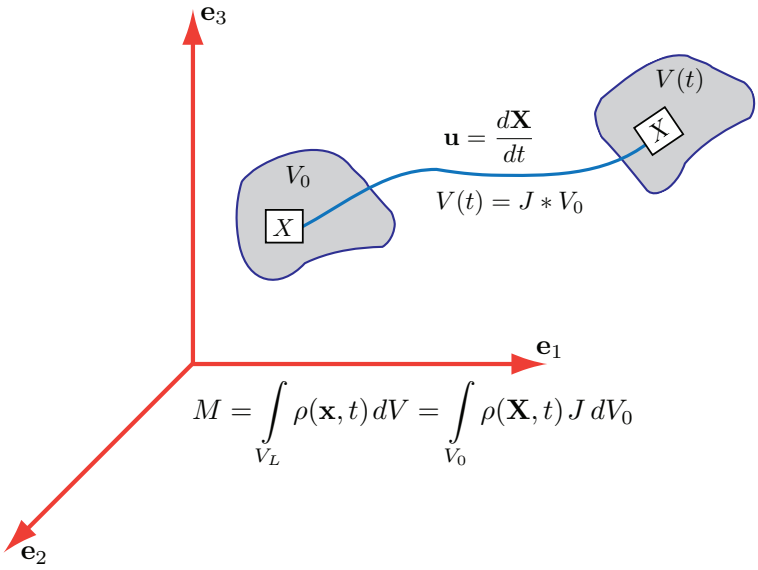

Fig. 1: The Lagrangian perspective. At $time = 0$ a volume of fluid, V_0, is identified. The volume is composed of a set of particles, $\mathbf{R}$, with each particle identified by its vector position $\mathbf{X}$. Even though the volume is sheared, rotated and dilated as it moves through space, it is always composed of the same set of particles $\mathbf{R}$. Thus, the boundary surrounding V is impermeable. The Jacobian, J, integrates the time-rate-of-change of V and represents the fractional change in the volume between $time = 0$ and $time = t$. The volume of fluid at any time t is equal to its volume at some initial time, V_0, times the fractional change in volume, J. Since the boundary of V is impermeable, the mass, M, within V is a constant in time.

The amount of mass, M, or tracer substance, Q, within the boundary surface can be expressed as

$$M = \int_{V(t)} \rho\,(\mathbf{x},t)\,dV \tag{1}$$

$$Q = \int_{V(t)} \rho\,(\mathbf{x},t)\,q\,(\mathbf{x},t)\,dV \tag{2}$$

where the limits of integration span the volume $V(t)$. The dependence of V on time is retained to make clear that the limits of integration, in general, change in time. ρ is the fluid density with units of *mass* per *volume* and q has units of concentration, such as *kg* of Q per *kg* of fluid.

Assume that no mass or tracer substance is exchanged across the boundary S such that

$$\frac{dM}{dt} = 0 \tag{3}$$

and

$$\frac{dQ}{dt} = 0. \tag{4}$$

Equation (3) and (4) define the material derivative as measured in the Lagrangian reference frame of motion by stating that the amount of M and Q is invariant in time when following a volume $V(t)$ that is always composed of the same set of particles included in **R**.

Another reference frame of great utility is the *Eulerian* reference frame where the observer remains at a fixed position in space, as opposed to moving in space along particle trajectories. The material derivative (of, say, Q) is expressed in the Eulerian reference frame as

$$\left.\frac{dQ}{dt}\right|_{fluid\ particle} \equiv \frac{DQ}{Dt} = \frac{\partial Q}{\partial t} + \mathbf{u}\cdot\nabla Q \tag{5}$$

where, as shown in Figure 1, $\mathbf{u}$ is the particle velocity defined as

$$\mathbf{u} = \frac{d\mathbf{X}}{dt}. \tag{6}$$

The gradient in (5) is define as

$$\nabla Q = \frac{\partial Q}{\partial x_1}\mathbf{e}_1 + \frac{\partial Q}{\partial x_2}\mathbf{e}_2 + \frac{\partial Q}{\partial x_3}\mathbf{e}_3. \tag{7}$$

Both terms on the right-hand side (RHS) of (5) are evaluated at a fixed time and at a fixed point. Even when the material derivative is identically zero, a non-zero time-rate of change, $\frac{\partial\{\}}{\partial t}$, can be observed at a fixed location due to the differential transport, $\mathbf{u}\cdot\nabla\{\}$, into and out-of a specific region. An Eulerian observer essentially balances $\frac{dM}{dt} = 0$ by measuring the differential transport at one location, then setting

the local time tendency to the value required to make the material derivative sum to zero.

The blending of the Lagrangian and Eulerian reference frames through the use of Arbitrary Lagrangian Eulerian (ALE) (Hirt et al, 1997) methods is increasingly popular in climate system modeling. While the full discussion of ALE methods is beyond the scope of this chapter, the analysis of the continuous system given in the following section can be extended to ALE frameworks.

3 Evolution Equations from a Lagrangian Perspective

The elegance and simplicity of the Lagragrian reference frame is clearly apparent in the equations (1) to (4). In a model of the global atmosphere or ocean we could envision decomposing the domain into a set of Lagrangian volumes where each volume is separated by an invisible, yet impermeable, barrier. The numerical algorithms would then track the ”blobs” as they move through space being pushed, squeezed and rotated due to their contact with neighboring blobs. In such a model the phenomena of transport would be remarkably well simulated; no mass or tracer substance would be erroneously exchanged between the Lagrangian volumes. In fact, ideas along these lines are under development by Haertel et al (2009) and Dixon and Ringler (2010, submitted).

The primary reason that no robust climate models are constructed entirely in a Lagrangian reference frame is due to the rapid deformation of the Lagrangian control volumes. As seen in Figure 1, while the mass within the volume V is constant in time, the volume itself can evolve in time through rotation, dilation and shearing. Figure 2 demonstrates what happens to control volumes in typical geophysical flows. Initially compact control volumes are stretched due to shearing. The stretching creates long filaments that are folded. Tracking these rapidly distorting control volumes poses a tremendous challenge for numerical modeling.

So while the Lagrangrian reference frame proves exceptionally useful for the construction of the evolution equations, numerical models are currently restricted to reference frames that are essentially Eulerian. As a result, we require a robust means of transforming conservation laws and evolution equations between the Lagrangian and Eulerian frames of motion. While several methodologies are available for transforming between these reference frames, an approach based on the Reynold’s Transport Theorem (RTT) is particularly appealing for two reasons. First, the RTT is formulated in an integral form that leads naturally to equations suitable to finite-volume models that will be discussed in Section 5 and 6. Second, a generalization of the RTT allows for the seamless transformation between the Lagrangian reference frame and any other reference frame that falls between the Lagragian (moving) and Eulerian (fixed) reference frame. Thus, the emerging type of models based on ALE methods are fully accommodated in approaches based on the RTT; this chapter serves as a useful waypoint on the path to developing numerical models in the ALE reference

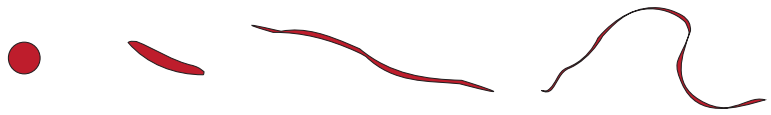

Fig. 2: In the highly nonlinear flows that characterize fluid motion in the atmosphere and ocean, Lagrangian control volumes are rapidly distorted due the presence of strong shear, rotation and dilation. The rapid distortion of Lagrangian control volumes makes the formulation of numerical models within the Lagrangian reference frame an extremely difficult challenge.

frame. A full analysis of RTT and its generalizations can be found in F. White's Fluid Mechanics textbook (White, 2008).

3.1 The Reynolds Transport Theorem

Let F be any intensive property of the fluid. Examples of F include ρ with units of mass per unit volume, ρq with units of tracer mass per unit volume or $\rho \mathbf{u}$ with units of momentum per unit volume. The conservation statement for F in the Lagrangian reference frame is expressed as

$$\frac{d}{dt}\left[\int_{V_L} F(\mathbf{x},t)\,dV\right] = 0. \tag{8}$$

Note that (3) is included as a specific example of (8).[1]

The subscript "L" on the volume V in (8) has been added to denote that the volume is being viewed by an observer moving in the Lagrangian reference frame. The goal is to move the time derivative inside the volume integral and, thereby, allow for the integration to occur over the same volume V but with respect to an observer in a different reference frame. This is somewhat problematic since the limits of integration, V_L, are a function of time.

The way around this difficulty is to make use of the fact that the volume V_L is composed of the same set of particles $\mathbf{R}$ at every instant in time. Thus, as shown in Figure 1, the differential volume element dV at some time t is related to its value at time $t = 0$ as

$$dV = J dV_0 \tag{9}$$

where J accounts for the fractional change in the volume element between time 0 and time t. Conceptually we can consider each of these differential fluid elements dV_0 as being associated with a single particle. Thus, (8) can be transformed to

$$\frac{d}{dt}\left[\int_{V_L} F(\mathbf{x},t)\,dV\right] = \frac{d}{dt}\left[\int_{V_0} F(\mathbf{X},t)\,J\,dV_0\right] = 0. \tag{10}$$

Note that both sides of (10) integrate over the same group of particles $\mathbf{R}$, but do so in different ways. The LHS indirectly sums over the particles by integrating over V_L, which is identical to spatial extent spanned by $\mathbf{R}$ at time t. The RHS explicitly sums over the particle positions $\mathbf{X}$ at time t included in V_L and weights each particle by its initial volume, V_0, times the fraction change in V_0 between $time = 0$ and $time = t$. Now that the limits of integration on the RHS are not a function of time, the order of integration and differentiation can be exchanged. In particular, we can write

$$\frac{d}{dt}\int_{V_0} F(\mathbf{X},t)\,J\,dV_0 = \int_{V_0}\left[J\,\frac{D}{Dt}F(\mathbf{X},t) + F(\mathbf{X},t)\frac{D}{Dt}J\right]dV_0 = 0. \tag{11}$$

Just as J accounts for the time-integrated factional change in the size of the volume elements, $\frac{DJ}{Dt}$ accounts for the instantaneous rate-of-change in the size of the volume elements, namely

$$\frac{DJ}{Dt} = J\,\nabla\cdot\mathbf{u}. \tag{12}$$

Equation (12) states that the rate-of-change of a Lagrangian volume (JV_0) is equal to its present volume (JV_0) times the divergence of the fluid; since V_0 is not a function of time it cancels in (11). Using (12) we can simplify (11) to

$$\int_{V_0}\left[\frac{D}{Dt}F(\mathbf{X},t) + F(\mathbf{X},t)\nabla\cdot\mathbf{u}\right]dV_0 = 0. \tag{13}$$

[1] In general the RHS of (8) need not be zero. A source term for F can be placed on the RHS of (8). The proper evaluation of this source term is along the volume trajectory.

We can expand the first term in (13) using the definition of the material derivative (5) and combine terms to obtain

$$\int_{V_0} \left[\frac{DF}{Dt} + F\nabla\cdot\mathbf{u} \right] dV_0 = \int_{V_0} \left[\frac{\partial F}{\partial t} + \nabla\cdot(F\,\mathbf{u}) \right] dV_0 = 0. \tag{14}$$

The broad utility and analytic power of (14) is in the choice of V_0. Note that the only requirements on V_0 are the following: V_0 is coincident with V_L at some instant in time and V_0 is fixed in space. Of particular interest is when V_L and V_0 *span the same volume of space* at the instant $time = 0$. At this instant in time, we can see that V_0 is the Eulerian representation of V_L, in that it spans the same volume but is not moving with the fluid. The volumes V_0 and V_L only differ in the reference frame of the observer, with the former in the Eulerian reference frame and the latter in the Lagrangian reference frame. Relabeling V_0 as V_E to emphasis this point[2], we can now write

$$\frac{d}{dt}\left[\int_{V_L} F(x,t)\,dV \right] = \int_{V_E} \left[\frac{\partial F}{\partial t} + \nabla\cdot(F\,\mathbf{u}) \right] dV = \int_{V_E} \left[\frac{DF}{Dt} + F\nabla\cdot\mathbf{u} \right] dV = 0. \tag{15}$$

Equation (15) is the Reynolds Transport Theorem (RTT).[3] The only way to satisfy (15) for any V_E is to guarantee that

$$\frac{\partial F}{\partial t} + \nabla\cdot(F\,\mathbf{u}) = 0. \tag{16}$$

A more useful form of (15) is obtained by applying the divergence theorem to the $\nabla\cdot(F\,\mathbf{u})$ term to yield

$$\frac{d}{dt}\left[\int_{V_L} F(\mathbf{x},t)\,dV \right] = \int_{V_E} \frac{\partial F}{\partial t} dV + \int_{S_E} F\,\mathbf{u}\cdot\mathbf{n}\,dS = 0 \tag{17}$$

where S_E is the surface bounding V_E and $\mathbf{n}$ is the unit vector normal to S_E directed outward. The RTT states that the time-rate-of-change of any intensive quantity F inside a volume V_L following the fluid motion can be computed at any instant in time as the sum of the time-rate-of-change of F inside V_E and the net flux of F across the surface bounding V_E. See Figure 3. The RTT allows for conservation statements

[2] The Eulerian volume, V_E, is often referred to as a "control volume" when discussed in the context of finite-volume methods

[3] The term "Reynolds Transport Theorem" is most commonly used when the volume V_L is transported with the fluid, as is the case for the first term in (15). When the volume is not being observed in the Lagrangian reference frame, a generalization of RTT still holds and that theorem is commonly referred to as the "Generalized Transport Theorem."

to be naturally cast in a integral form[4] as shown in (17). With the machinery of the RTT in place, we can easily apply it to any conservation statement to obtain an analytic expression of the dynamical core expressed in integral form.

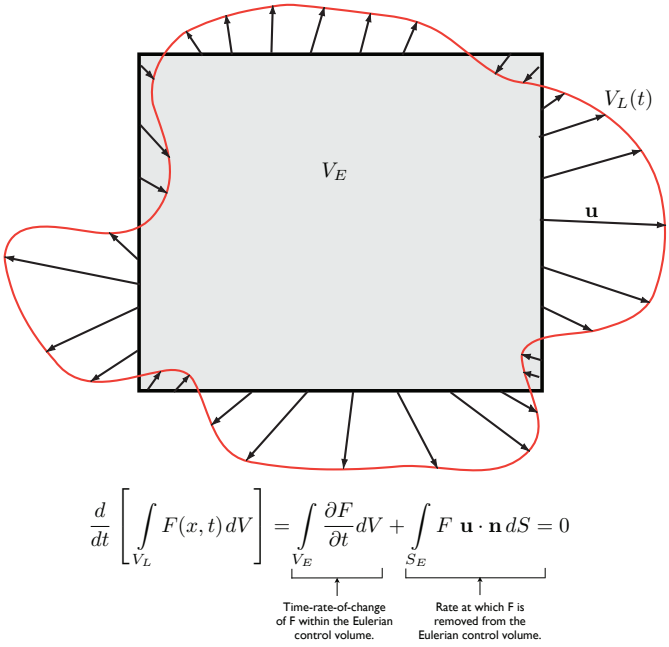

Fig. 3: An illustration of the Reynolds Transport Theorem. At some time $t = 0$, the volume V_L is coincident with the volume V_E. The Eulerian volume V_E remains fixed in place while the Lagrangian volume V_L deforms to $V_L(t)$ at time t. The conservation statement for F is that the integral of $F\,dV$ over V_L is constant for all time. The Reynolds Transport Theorem allows for the computation of the time-rate-of-change for F within V_E by computing the flux of F that is transported across V_E over time t.

3.2 Conservation of Mass and Tracer Substance

Applying (17) to the conservation of mass and tracer expressions in (3) and (4), we obtain

[4] The *integral form* is also referred to as the *weak form* since, in general, the statements hold only for a compact region of integration.

$$\frac{d}{dt}\left[\int_{V_L}\rho dV\right]=\int_{V_E}\frac{\partial\rho}{\partial t}dV+\int_{S_E}\rho\,\mathbf{u}\cdot\mathbf{n}dS=0, \tag{18}$$

$$\frac{d}{dt}\left[\int_{V_L}\rho q dV\right]=\int_{V_E}\frac{\partial(\rho q)}{\partial t}dV+\int_{S_E}\rho q\,\mathbf{u}\cdot\mathbf{n}dS=0. \tag{19}$$

Equations (18) and (19) are inextricably coupled and a discussion of the coupling is worthy of its own chapter. A glimpse at this entanglement can be seen by simply defining $G_m=\rho\,\mathbf{u}\cdot\mathbf{n}$ and rewriting (18) and (19) as

$$\frac{d}{dt}\left[\int_{V_L}\rho dV\right]=\int_{V_E}\frac{\partial\rho}{\partial t}dV+\int_{S_E}G_m\,dS=0, \tag{20}$$

$$\frac{d}{dt}\left[\int_{V_L}\rho q dV\right]=\int_{V_E}\frac{\partial(\rho q)}{\partial t}dV+\int_{S_E}q\,G_m\,dS=0. \tag{21}$$

G_m is the mass flux per unit area across S_E. Equation (21) shows that a prerequisite to computing the tracer flux across S_E is the knowledge of the mass flux G_m. In fact, when written in this manner it is clear that tracer transport is meaningless without the underlying mass transport field G_m. Those transport algorithms that fully recognize the relationship between mass and tracer transport are most appropriate for use in climate simulations.

Differential forms of mass and tracer transport can be obtained directly from (16) or by letting $V_E\rightarrow 0$ in (18) and (19) to obtain

$$\frac{\partial\rho}{\partial t}+\nabla\cdot(\rho\,\mathbf{u})=0 \tag{22}$$

and

$$\frac{\partial(\rho q)}{\partial t}+\nabla\cdot(\rho q\,\mathbf{u})=0. \tag{23}$$

Equations (22) and (23) can be written in material derivative form as

$$\frac{D\rho}{Dt}+\rho\nabla\cdot\mathbf{u}=0 \tag{24}$$

and

$$\frac{Dq}{Dt}=0 \tag{25}$$

The last two forms will be used in the discussion below.

3.3 A Statement of Newton's Second Law

In order to complete the Lagrangian perspective illustrated in Figure 1, we need to describe how the volume evolves in time, i.e. what determines the set of particle velocities $\mathbf{u}$ that will dilate, rotate and shear the volume V_L shown in Figure 1? In this case the intensive quantity is momentum per unit volume,

$$\mathbf{P} = \rho\,\mathbf{u}. \tag{26}$$

In its most basic form, the statement of Newton's Second Law is

$$\frac{d\mathbf{P}}{dt} = \frac{d}{dt}\left[\int_{V_L} \mathbf{P}(\mathbf{x},t)\,dV\right] = \int_{V_L} \mathbf{F}_b\,dV + \int_{S_L} \mathbf{F}_s\,dS \tag{27}$$

where $\mathbf{F}_b$ is a *body force* acting throughout the volume V_L and $\mathbf{F}_s$ is a *surface force* acting on the surface S_L. $\mathbf{F}_b$ has units of force per unit volume and $\mathbf{F}_s$ has units of force per unit area. Applying RTT as expressed in (13) to (27) yields

$$\int_{V_E} \left[\frac{D}{Dt}(\rho\,\mathbf{u}) + (\rho\,\mathbf{u})\nabla\cdot\mathbf{u}\right] dV = \int_{V_E} \mathbf{F}_b\,dV + \int_{S_E} \mathbf{F}_s\,dS. \tag{28}$$

Expanding the material derivative and combining terms results in

$$\int_{V_E} \left[\rho\frac{D\mathbf{u}}{Dt} + \mathbf{u}\left(\frac{D\rho}{Dt} + \rho\nabla\cdot\mathbf{u}\right)\right] dV = \int_{V_E} \mathbf{F}_b\,dV + \int_{S_E} \mathbf{F}_s\,dS. \tag{29}$$

The term $\left(\frac{D\rho}{Dt} + \rho\nabla\cdot\mathbf{u}\right)$ is a statement of conservation shown in (24) and is identically zero. The momentum equation now has a form that is analogous to $m\mathbf{a} = \mathbf{F}$ with

$$\int_{V_E} \rho\frac{D\mathbf{u}}{Dt}\,dV = \int_{V_E} \mathbf{F}_b\,dV + \int_{S_E} \mathbf{F}_s\,dS \tag{30}$$

where $\frac{D\mathbf{u}}{Dt}$ is exactly equal to the particle acceleration. The specific forces that are applied to the RHS can range from the Coriolis force[5] to the pressure gradient force to surface drag to shear stress, just to name a few. The focus here will be on the forces responsible for geostrophic balance: Coriolis and pressure. In addition, the Coriolis force is representative of a body force with the integration over V_E, and the pressure force is representative of a surface force with the integration over S_E. The Coriolis force can be expressed as

[5] The Coriolis force is an *apparent* force that arises due to casting the equations of motion in a non-inertial, rotating reference frame. Both the Lagrangian and Eulerian reference frames are measured relative to the underlying rotating reference frame. If the system of equations were cast in an inertial reference frame, then the Coriolis "force" would not be present.

$$\int_{V_E} \mathbf{F}_b \, dV = -\int_{V_E} f_o \, \mathbf{k} \times (\rho \, \mathbf{u}) \, dV \tag{31}$$

where f_o is the Coriolis parameter that is assumed to be a constant (i.e. a *f-plane* approximation has been assumed) and $\mathbf{k}$ is the unit vector pointing in the local vertical direction. The pressure force can be expressed as

$$\int_{S_E} \mathbf{F}_s \, dS = -\int_{S_E} p \, \mathbf{n} \, dS = -\int_{V_E} \nabla p \, dV \tag{32}$$

where $\mathbf{n}$ is the outward directed normal vector to S_E. The negative sign on the $p\,\mathbf{n}$ term in (32) is because, by definition, pressure "pushes" inward on S_E resulting in a force directed in the $-\mathbf{n}$ direction. Equation (32) also uses the divergence theorem to transform the pressure force from an integral over S_E to an integral over V_E.

Letting $V_E \to 0$ allows (30) to be expressed in its differential form as

$$\frac{D\mathbf{u}}{Dt} = -f_o \, \mathbf{k} \times \mathbf{u} - \frac{1}{\rho} \nabla p. \tag{33}$$

One numerical method that will be of particular interest below is the "finite-volume approach." In this approach, we retain prognostic equations for *mean values* over discrete regions. As a result, the weak or integral form of (33) is more amenable to a finite-volume approach. In order manipulate the momentum equation shown in (33) into weak form, we can apply (17) to the intensive quantity $P = \rho \, \mathbf{u}$ to obtain

$$\int_{V_E} \frac{\partial (\rho \, \mathbf{u})}{\partial t} dV + \int_{S_E} (\rho \, \mathbf{u}) \, \mathbf{u} \cdot \mathbf{n} dS = \int_{V_E} \mathbf{F}_b \, dV + \int_{S_E} \mathbf{F}_s \, dS. \tag{34}$$

With examples of $\mathbf{F}_b$ and $\mathbf{F}_s$ in place, the integral form of the momentum equation becomes

$$\int_{V_E} \frac{\partial (\rho \, \mathbf{u})}{\partial t} dV + \int_{S_E} (\rho \, \mathbf{u}) \, \mathbf{u} \cdot \mathbf{n} dS = -\int_{V_E} f_o \, \mathbf{k} \times (\rho \, \mathbf{u}) \, dV - \int_{S_E} p \, \mathbf{n} \, dS. \tag{35}$$

Figure 4 illustrates the various terms involved in (35). Allowing $V_E \to 0$ in (35) and transforming the 2nd and 4th term using the divergence theorem gives

$$\frac{\partial (\rho \, \mathbf{u})}{\partial t} + \nabla \cdot (\rho \, \mathbf{u} \, \mathbf{u}) = -f_o \, \mathbf{k} \times (\rho \, \mathbf{u}) - \nabla \cdot p. \tag{36}$$

We have developed several different analytic forms of $\mathbf{F} = m \, \mathbf{a}$ in this section. In particular, a particle-based formulation of momentum is shown in (33) and a control-volume formulation is shown in (35). When constructing a numerical model, each form will have its own advantages and disadvantages. We will return to this discussion in Section 4.

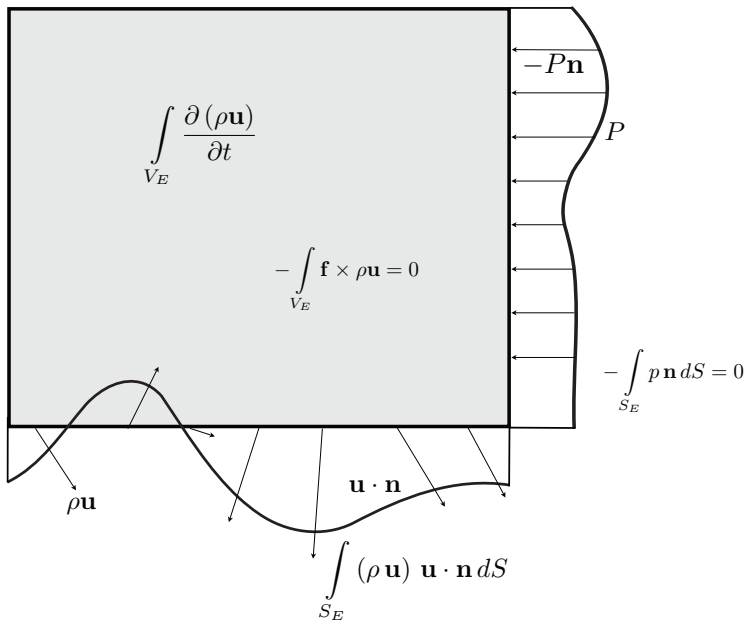

Fig. 4: A control volume perspective of conservation of momentum: The time-rate-of-change of momentum, $\rho\mathbf{u}$, within V_E is due to three mechanisms. The first is the apparent body force, $-f_o\mathbf{k}\times\mathbf{u}$, acting over the entire control volume V_E. The second is due to the pressure force acting along the boundary of V_E. And the last mechanism is the transport of momentum, $\rho\mathbf{u}$, across the boundary of V_E. Other mechanisms such as dissipation and external sources can also be included.

3.4 Dynamics of Vorticity

By using $\mathbf{F} = m\mathbf{a}$ to construct the evolution equation for velocity or momentum, we are describing how a particle (33) or a region of fluid (35) responses to applied forces. In addition to the balance-of-forces in the momentum equation, there are *kinematic* constraints on the structure of the velocity field. A vector velocity field can always be described as a sum of two vector velocity fields where one vector field is purely rotational and the other vector field is purely divergent. This is known as the Helmoltz Decomposition[6]. The Helmoltz Decomposition states that we can always decompose a vector field as

$$\mathbf{u} = \mathbf{u}_\delta + \mathbf{u}_\zeta \tag{37}$$

[6] The simplification to singly-connected domains extending to infinity is made here for clarity in presentation, see (Batchelor, 1967) page 85 for a full discussion.

with

$$\nabla \cdot \mathbf{u} = \nabla \cdot \mathbf{u}_\delta = \delta, \tag{38}$$

and

$$\nabla \times \mathbf{u} = \nabla \times \mathbf{u}_\zeta = \zeta, \tag{39}$$

where δ is the scalar divergence field associated with $\mathbf{u}$ and ζ is the vector vorticity field associated with $\mathbf{u}$. Equations (38) and (39) show that the divergent component of $\mathbf{u}$ is contained entirely in $\mathbf{u}_\delta$ and the rotational component of $\mathbf{u}$ is contained entirely in $\mathbf{u}_\zeta$. Given a divergence and vorticity field, the velocity field can be determined by first finding the potential fields consistent with δ and ζ as

$$\nabla^2 \phi = \delta, \tag{40}$$

and

$$\nabla^2 \beta = \zeta \tag{41}$$

and then differentiating the potential fields to obtain the velocities as

$$\nabla \phi = \mathbf{u}_\delta, \tag{42}$$

and

$$\nabla \times \beta = \mathbf{u}_\zeta \,. \tag{43}$$

Solving (40) and (41) for the potential fields requires the inversion of the ∇^2 operator.[7] While the Helmoltz Decomposition holds for three-dimensional flows, we will limit the velocity to 2-D planar flows in the following section.

Broadly speaking, the rotational component of the velocity field, $\mathbf{u}_\zeta$, is associated with slow modes, such as Rossby waves, and the divergent component of the velocity field, $\mathbf{u}_\delta$, is associated with fast modes, such as gravity waves. An adequate representation of both the rotational and divergent components of motion is a prerequisite to robust simulations of geophysical fluid dynamics.

From a climate modeling perspective, avoiding the spurious forcing of the rotational component of the velocity field is of great concern. Since the vorticity field tends to evolve slowly in time via transport (i.e. it is a slow mode), errors in the evolution of the rotational component of velocity tend to be advected along with the fluid flow and, thus, accumulate in time. Discrete numerical models with spurious forcing of the vorticity field resort, inevitably, to inappropriately large levels of dissipation in order to control the spurious accumulation of vorticity variance at the model grid-scale.

Throughout the remaining sections of this chapter a tremendous amount of discussion will focus how to design numerical methods that appropriately solve $\mathbf{F} = m\,\mathbf{a}$ while avoiding any spurious forcing of the vorticity field. We will begin this discussion by developing conservation statements in the continuous system regarding how

[7] In singly-connected domains, like the entire surface of the sphere, no additional boundary conditions are required to solve (40) and (41). In multi-connected domains, additional boundary conditions are required to close the system.

the rotational component of the velocity field *should* evolve in time. Later sections will focus on how to build these conservation statements into the discrete system.

3.4.1 Conservation of Circulation

Circulation measures the mean rotation around a material contour (see Figure 5). Circulation is essentially the area-weighted representation of vorticity. In the discussion of circulation and vorticity, we will limit the velocity field to two spatial directions, such as the surface of a plane. The reduction in the space spanned by the velocity field means that volume integrals in RTT reduce to surface integrals and surface integrals in RTT reduce to contour integrals. The *relative* circulation is defined as

$$\Gamma^r_{c(t)} = \oint_{c(t)} \mathbf{u}\cdot\mathbf{dr} = \int_{S(t)} (\nabla\times\mathbf{u})\cdot\mathbf{n}\,dS = \int_{S(t)} \zeta\cdot\mathbf{n}\,dS \tag{44}$$

where $\Gamma^r_{c(t)}$ measures the mean rotation produced by the velocity field $\mathbf{u}$ around a $c(t)$ that moves with the material particles. Here $\mathbf{n}$ is the outward directed normal to dS; for the 2D system considered here $\mathbf{n}$ is the local vertical, thus $\zeta\cdot\mathbf{n}$ measures the component of vorticity in the vertical direction. The limits of integration are around the contour $c(t)$, or over the area $S(t)$ associated with the contour. The explicit dependence on time has been retained in $c(t)$ and $S(t)$ to emphasize that the limits of integration are a function of time. All analysis in this section will take place in the Lagrangian reference frame; the use of RTT to transform the conservation statements to the more practical Eulerian reference frame will be done in the following section.

The first task is to determine the appropriate conservation statement for circulation within a Lagrangian control area. Note that since the contour of integration in (44) moves with the fluid, the contour is composed of the same set of particles for all time. Applying the time derivative to (44) yields

$$\frac{d}{dt}\Gamma^r_{c(t)} = \frac{d}{dt}\oint_{c(t)} \mathbf{u}\cdot\mathbf{dr} = \oint_{c(t)} \left[\mathbf{dr}\cdot\frac{d\,\mathbf{u}}{dt}\bigg|_{particle} + \mathbf{u}\cdot\frac{d\,(\mathbf{dr})}{dt}\right]. \tag{45}$$

Since the element $\mathbf{dr}$ is transported with velocity $\mathbf{u}$, its time-rate-of-change can be expressed as

$$\frac{d\,(\mathbf{dr})}{dt} = \mathbf{dr}\cdot(\nabla\mathbf{u})\,. \tag{46}$$

The RHS of (46) measures the deformation and rotation of $\mathbf{dr}$ due to spatial variations in the $\mathbf{u}$ field.[8] Using (46) in (45) yields

[8] Equation (46) is obtained by noting that $\frac{d(\mathbf{dr})}{dt} = \mathbf{u}(\mathbf{x}+\mathbf{dr}) - \mathbf{u}(\mathbf{x})$, expanding $\mathbf{u}(\mathbf{x}+\mathbf{dr})$ in a Taylor series and retaining the first two terms.

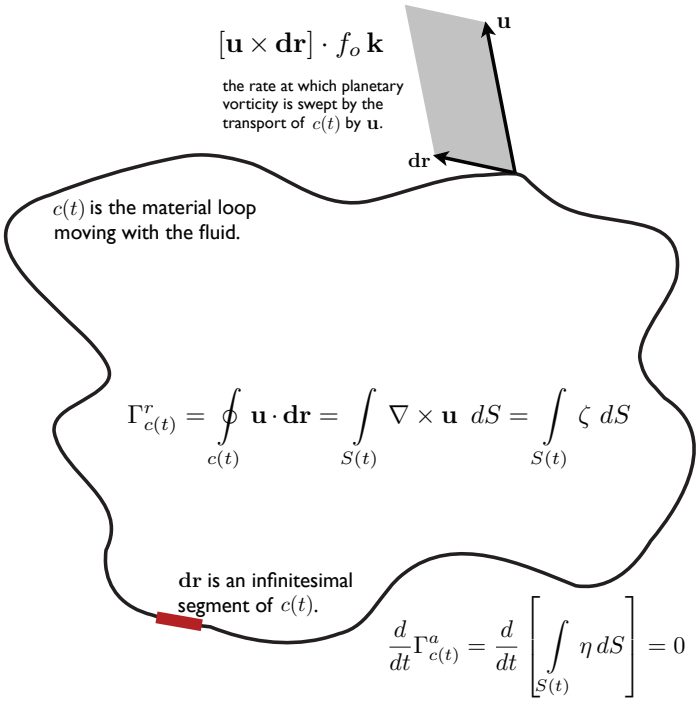

Fig. 5: A graphical representation of circulation.

$$\frac{d}{dt}\Gamma^r_{c(t)} = \oint_{c(t)} \left[\frac{D\mathbf{u}}{Dt} + \nabla\left(\frac{|\mathbf{u}|}{2}\right)\right] \cdot \mathbf{dr} = \oint_{c(t)} \frac{D\mathbf{u}}{Dt} \cdot \mathbf{dr} \tag{47}$$

where (5) is used to recast the time derivative of $\mathbf{u}$ as a material derivative. The relationship between the evolution of circulation and $\mathbf{F} = m\mathbf{a}$ is becoming apparent with the appearance of the $\frac{D\mathbf{u}}{Dt}$ in (47). If we substitute in the form of the momentum equation defined in (33) we obtain

$$\frac{d}{dt}\Gamma^r_{c(t)} = \oint_{c(t)} \left[-f_o \, \mathbf{k} \times \mathbf{u} - \frac{\nabla p}{\rho}\right] \cdot \mathbf{dr}. \tag{48}$$

The first source of relative circulation on the RHS of (48) is related to the amount of planetary vorticity "captured" in $c(t)$ due to expansion or contraction of the area associated with $c(t)$. Referring to Figure 5 we can manipulate this source term as

$$-\oint_{c(t)} [f_o \mathbf{k} \times \mathbf{u}] \cdot \mathbf{dr} = -\oint_{c(t)} [\mathbf{u} \times \mathbf{dr}] \cdot f_o \mathbf{k} = -f_o \frac{D}{Dt} S(t) = -\frac{D}{Dt} [f_o S(t)]. \quad (49)$$

The term $\mathbf{u} \times \mathbf{dr}$ represents the rate at which area is swept by the transport of element $\mathbf{dr}$ by velocity $\mathbf{u}$. When integrated around the entire contour and multiplied by the planetary vorticity, the result measures the time-rate-of-change in the amount of planetary vorticity contained within $c(t)$. If we define the *planetary* circulation as

$$\Gamma^p_{c(t)} = f_o S(t) \quad (50)$$

then we can express the *absolute* circulation as

$$\Gamma^a_{c(t)} = \Gamma^r_{c(t)} + \Gamma^p_{c(t)} = \int_{S(t)} (\zeta + f_o)\, dS = \int_{S(t)} \eta\, dS \quad (51)$$

where η is the absolute vorticity defined as the sum of the relative vorticity and the planetary vorticity. We can now rewrite (48) as

$$\frac{d}{dt} \Gamma^a_{c(t)} = \oint_{c(t)} \left[-\frac{\nabla p}{\rho} \right] \cdot \mathbf{dr} \quad (52)$$

where (52) is an expression for the rate-of-change of absolute circulation associated with a contour $c(t)$ that is observed in the Lagrangian reference frame. The remaining source term on the RHS of (52) is the due to the differential acceleration of particles along $c(t)$ produced by the pressure gradient force when variations in the density field are present. The primary interest here is on the situation when the density field is constant[9], i.e. $\rho = \rho_o$. In this situation we find

$$\oint_{c(t)} \left[-\frac{\nabla p}{\rho_o} \right] \cdot \mathbf{dr} = \frac{-1}{\rho_o} \oint_{c(t)} \nabla p \cdot \mathbf{dr} = 0. \quad (53)$$

The term $\nabla p \cdot \mathbf{dr}$ measures the gradient of the pressure field in the direction of $\mathbf{dr}$. So long as the $c(t)$ loop traced out by the differential $\mathbf{dr}$ elements is closed, the integration of $\nabla p \cdot \mathbf{dr}$ around $c(t)$ is guaranteed to be identically zero. This results holds for any loop and for any scalar field. With the result provided in (53), we can end the analysis with

[9] When variations in density are present, as in the real atmosphere and ocean, then the RHS of (52) serves as a source of vorticity. When considering the numerical simulation of this process, a critical prerequisite is the guarantee that vorticity is *not* created when these variations are *not* present.

$$\frac{d}{dt}\Gamma^a_{c(t)} = \frac{d}{dt}\left[\int_{S(t)} \eta\, dS\right] = 0 \tag{54}$$

that states that the absolute circulation contained within contour $c(t)$ as it moves with the fluid will be a constant in time; absolute circulation within $c(t)$ is conserved in time. The relationship also makes clear that, in general, the absolute vorticity *is not* constant within the contour $c(t)$. Only in the special case of non-diverengent flow resulting in $\frac{D}{Dt}[S(t)] = 0$ will the mean value of η be a constant within contour $c(t)$.

3.4.2 Conservation of Absolute Vorticity

The entire analysis in the section above is conducted in the Lagrangian reference frame. The purpose of this section is to use RTT to transfer the conservation statements into an Eulerian reference frame. Comparing (54) to (8) shows that the form of conservation of absolute circulation shown in (54) is suitable for the application of RTT. Applying RTT as stated (15) to (54), we find

$$\frac{d}{dt}\Gamma^a_{c(t)} = \frac{d}{dt}\left[\int_{S(t)} \eta\, dS\right] = \int_S \left[\frac{\partial \eta}{\partial t} + \nabla\cdot(\eta\ \mathbf{u})\right] dS = 0. \tag{55}$$

The form of (55) that is most suitable to finite-volume applications discussed below is

$$\int_S \frac{\partial \eta}{\partial t} dS + \oint_c \eta\ \mathbf{u}\cdot\mathbf{n}\, dr = 0 \tag{56}$$

that states that the time-tendency of absolute vorticity in region S is equal and opposite to the rate at which absolute vorticity is being transported out of region S. A primary goal in the construction of the numerical model developed below is to guarantee that the velocity field evolves in such a way as to mimic (56) exactly.

For the sake of completeness we note that in the limit of $dS \to 0$ and allowing ρ to be nonuniform, (55) becomes

$$\frac{\partial \eta}{\partial t} + \nabla\cdot(\eta\ \mathbf{u}) = -\nabla\times\left[\frac{\nabla p}{\rho}\right] \tag{57}$$

where the RHS source term shown in (52) has been retained. And finally, introducing the material derivative into (58) yields

$$\frac{D\eta}{Dt} + \eta\nabla\cdot\mathbf{u} = -\nabla\times\left[\frac{\nabla p}{\rho}\right]. \tag{58}$$

3.5 Summary of Evolution Equations

The analytic analysis of the continuous system is now complete. The approach has been to identify conservation statements in the Lagrangian reference frame and to use the Reynolds Transport Theorem to transfer these conservation statements into an Eulerian reference frame. The value of the Reynolds Transport Theorem is that it provides a machine-like approach to the derivation of evolution equations specified naturally in the integral form conducive to the development of finite-volume methods.

Before turning to the process of discretization, a survey is conducted of the various flavors of $\mathbf{F} = m\mathbf{a}$ that can be used as the basis, or starting point, for the discretization process. The specific form of $\mathbf{F} = m\mathbf{a}$ that is chosen as the starting point for the numerical model has a tremendous impact on the attributes of that numerical model. Particular attention is paid to the ability of each form to satisfy both $\mathbf{F} = m\mathbf{a}$ and conservation of absolute vorticity (56).

4 The Various Flavors of $\mathbf{F} = m\mathbf{a}$

In the continuous system, all forms of the momentum equation are equivalent.[10] Since each form can be manipulated into any other form, there is no difference between the various expressions of $\mathbf{F} = m\mathbf{a}$. This is not true in the setting of discrete numerics. Discretizing the continuous system implies the approximation of the continuous fields as a finite set of values that typically exist on a mesh that spans the spatial extent of the system. In addition, the continuous operators such as ∇, $\nabla\cdot$ and $\nabla\times$ are replaced with discrete approximations. One result of discretizing the momentum equation is that the various forms are no longer equivalent; we can not, in general, manipulate one discrete form of the momentum equation into another discrete form using the discrete operators. As a result, when we choose the form of the momentum equation used in a numerical model, we are saying a great deal about what aspects of $\mathbf{F} = m\mathbf{a}$ are most important in the target application. Each form has its own advantages and disadvantages and, thus, each form has its own niche to fill in the modeling of the global atmosphere and ocean systems. This section provides a brief review of the commonly used flavors of $\mathbf{F} = m\mathbf{a}$ with a discussion of their respective advantages and disadvantages.

4.1 The Advective Form

The advective form of the momentum equation (33) is restated here for convienence:

[10] The equivalence holds for smooth flows. If singularities development in the solution, the equivalence between the various forms is more tenuous.

$$\frac{D\mathbf{u}}{Dt} = -f_o\,\mathbf{k}\times\mathbf{u} - \frac{1}{\rho}\nabla\cdot p. \tag{59}$$

This is essentially an evolution equation for one of the particles in the Lagrangian system, such as particle $\mathbf{X}$ shown in Figure 1. Assume that the system is discretized on a regular mesh composed of squares, such as the one shown in Figure 6. If at some time, say $t = t_b$ one particle is placed at the center of each square shown in Figure 6, then the particle position and velocity at some later time, say $t = t_e$, is determined by integrating (59) *along the particle trajectory* as

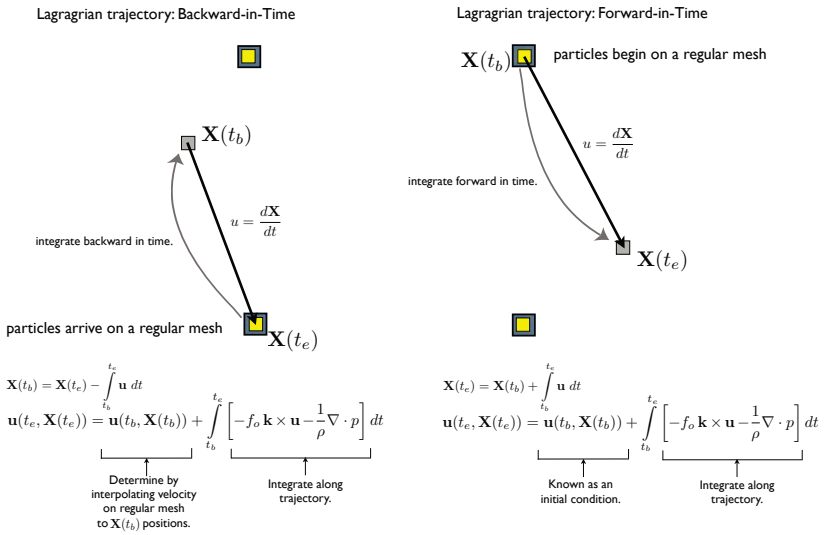

Fig. 6: A graphical representation of forward Lagrangian and backward Lagrangian (i.e. the semi-Lagrangian) method.

$$\int_{t_b}^{t_e} \frac{D\mathbf{u}}{Dt} = \mathbf{u}(t_e, \mathbf{X}(t_e)) - \mathbf{u}(t_b, \mathbf{X}(t_b)) = \int_{t_b}^{t_e} \left[-f_o\,\mathbf{k}\times\mathbf{u} - \frac{1}{\rho}\nabla\cdot p\right] dt. \tag{60}$$

Assuming that the particle positions and velocities are known at t_b, the system is solved for $\mathbf{X}(t_e)$ and $\mathbf{u}(\mathbf{X}(t_e), t_e)$ as

$$\mathbf{X}(t_e) = \mathbf{X}(t_b) + \int_{t_b}^{t_e} \mathbf{u}\, dt, \tag{61}$$

$$\mathbf{u}(t_e, \mathbf{X}(t_e)) = \mathbf{u}(t_b, \mathbf{X}(t_b)) + \int_{t_b}^{t_e} \left[-f_o\, \mathbf{k} \times \mathbf{u} - \frac{1}{\rho} \nabla \cdot p \right] dt. \tag{62}$$

It needs to be emphasized that all of the source-term integrals on the RHS of (62) are along the particle path starting at time t_b at position $\mathbf{X}(t_b)$ and ending at time t_e at position $\mathbf{X}(t_e)$. While there are certainly challenges with the discrete evaluation of the RHS of (62), a more basic problem with the approach is that the particle positions at the end of the time step are, in general, no longer on a regular mesh (see Figure 6). More forward-in-time steps will lead to a continual distortion of particle positions due to the same shearing, stretching and deformation mechanisms illustrated in Figure 2. In order to prevent this continual distortion, (60) is generally evaluated *backward in time* in what is commonly known as the *semi-Lagrangian approach* (see Staniforth and Cote (1991) for a complete review).

Instead of assuming that the particles exist on a regular mesh at the beginning of the time step, the particles are assumed to reside on the regular mesh at the end of the time step. In this situation, the particle positions $\mathbf{X}(t_e)$ are required to form the regular mesh shown in Figure 6. The challenge is then to determine $\mathbf{X}(t_b)$ by integrating particle trajectories backward in time, i.e. to determine the starting point of the particles such that the particles "arrive" on a regular mesh at t_e. In this approach the system is solved for $\mathbf{X}(t_b)$ and $\mathbf{u}(\mathbf{X}(t_e), t_e)$ as

$$\mathbf{X}(t_b) = \mathbf{X}(t_e) - \int_{t_b}^{t_e} \mathbf{u}\, dt, \tag{63}$$

$$\mathbf{u}(t_e, \mathbf{X}(t_e)) = \mathbf{u}(t_b, \mathbf{X}(t_b)) + \int_{t_b}^{t_e} \left[-f_o\, \mathbf{k} \times \mathbf{u} - \frac{1}{\rho} \nabla \cdot p \right] dt. \tag{64}$$

In general, $\mathbf{u}(t_b, \mathbf{X}(t_b))$ is determined by interpolating the velocity values known on the fixed mesh at time t_b to $\mathbf{X}(t_b)$ locations. Equation (63) and (64) are coupled and need to be solved jointly or iteratively. The challenges of evaluating the RHS along the particle trajectory still remain.

The advantage of this approach is that exceptionally long time steps are possible.[11] Since the integration is occurring along the particle characteristic, traditional advective CFL time step constraints do not apply. An additional advantage is the ease with which tracer constituents can be updated. Using (25) and integrating $\frac{Dq}{Dt}$ from t_b to t_e, we have

[11] While longer time steps reduce the computational expense of a given simulation, longer time steps also often lead to less accurate results. Weighing the relative value of "fast" versus "correct" is important in choosing the time step for a simulation.

$$q(t_e, \mathbf{X}(t_e)) = q(t_b, \mathbf{X}(t_b)). \tag{65}$$

$q(t_b, \mathbf{X}(t_b))$ is determined by interpolating the tracer values from the regular mesh to the departure points $\mathbf{X}(t_b)$. Once this interpolation is complete, the updated tracer values are known immediately since q is conserved along particle trajectories.

The disadvantages in this approach to solving the momentum equation are related to the lack of conservation of mass and tracer substance and the spurious generation of vorticity. While these disadvantages pose severe problems in the context of long-time simulations typical in climate applications, these disadvantages have been successfully mitigated and/or circumvented for numerical weather prediction applications where the integration time scales are on the order of days to a week or two. Another alternative is to abandon the particle-centric approach of pure semi-Lagrange schemes and move to a cell-based approach. [check; cross reference Peter's chapter]

The issues regarding conservation can be readily identified by comparing (65) to (4). The conservation statement is that the mass-weighted integral of q (i.e. Q) is conserved in time when no sources or sinks are present. Yet (65) only "sees" the tracer concentration q for an isolated number of particles and, furthermore, that concentration is computed at locations $\mathbf{X}(t_b)$ via an interpolation procedure where accuracy is generally much more important than conservation.

The issues regarding spurious vorticity generation are equally problematic in the context of climate system modeling. In general, getting a handle on the evolution of vorticity in a particle formulation is extremely difficult. Using (58) we could certainly "tag" each particle with an associated vorticity, but the evolution of absolute vorticity during the time step involves spatial gradients that are difficult to compute. In addition, the same issue regarding lack of conservation occurs in the context of vorticity as occurs in the context of tracer transport. And finally, even if one could manage to evolve vorticity with the particles in a realistic manner, it is not clear how that information could be used to control the evolution of the prognostic velocity field shown in (64).

4.2 The Flux Form

The flux form of the momentum equation is shown in (34), illustrated in Figure 4 and rewritten here for 2D planar flow as

$$\int_{S_E} \frac{\partial(\rho\,\mathbf{u})}{\partial t} dS + \int_{c_E} (\rho\,\mathbf{u})\,\mathbf{u}\cdot\mathbf{n}\,dc = -\int_{S_E} f_o\,\mathbf{k}\times(\rho\,\mathbf{u})\,dS - \int_{c_E} p\,\mathbf{n}\,dc. \tag{66}$$

The main advantage of the flux-form momentum equation is that it is relatively easy to insure that the transport of momentum (the 2nd term in (66)) is conservative, i.e. momentum that exits one cells across c_E enters a neighbor cell. This same conservation property occurs in the evaluation of the pressure force; along a contour

c_E the pressure force results in an equal and opposite source of momentum for the surfaces that share c_E. An additional advantage of the flux-form is that density is incorporated into the prognostic variable. When using the flux-form of momentum, the prognostic variable is $\rho\,\mathbf{u}$, whereas all the other forms have $\mathbf{u}$ as the prognostic variable. The merit in retaining $\rho\,\mathbf{u}$ as the prognostic variable is that as $\rho \rightarrow 0$ the prognostic variable goes to zero so long as $\mathbf{u}$ remains bounded. In the emerging class of atmosphere and ocean models, ρ is often related to the vertical layer thickness, so $\rho \rightarrow 0$ is equivalent to a layer collapsing to zero thickness when all of the mass in a given layer at a given position is evacuated (e.g. Konor and Arakawa (1997) and Bleck and Smith (1990)). This is a common occurrence in numerical models and the flux-form momentum equation provides ample opportunities to insure that the discrete system remains well-behaved even in the the presence of "massless" layers.

The primary disadvantage in the use of the flux-form momentum equation is that the curl of (66) does not lead directly to a vorticity equation; vorticity and circulation are purely kinematic quantities that are related to the $\nabla \times \mathbf{u}$ not $\nabla \times (\rho\,\mathbf{u})$. As a result, discrete models based on the flux-form of the momentum equation do not conserve vorticity. In a discrete formulation of (66) every term has the potential to generate spurious vorticity. If no guarantees can be provided in regards to the conservation of circulation or vorticity, in general the only recourse is to increase the level of dissipation to maintain a regular, well-behaved solution. If the level of dissipation required to suppress the spurious generation of vorticity is significantly higher than is physically warranted, one should expect the numerical simulation to be degraded due to the physically-excessive dissipation.

The spurious generation of vorticity is due to errors in the discretization of the system. Assuming smooth flows, these errors approach zero as the order-of-accuracy of the discrete operators is increased and/or as the grid resolution is increased. The possibility certainly exists that these spurious errors are acceptably small, even for climate simulations, when employing high-order numerical methods and/or high-resolution meshes.

4.3 The Vector-Invariant Form

The vector-invariant form is derived from the advective form (59) where the material derivative is expanded into time tendency and transport terms using (5) to obtain

$$\frac{\partial \mathbf{u}}{\partial t} + (\mathbf{u}\cdot\nabla)\,\mathbf{u} = -f_o\,\mathbf{k}\times\mathbf{u} - \frac{1}{\rho}\nabla\cdot p. \tag{67}$$

If the $(\mathbf{u}\cdot\nabla)\,\mathbf{u}$ term is replaced based on the following vector identity

$$(\mathbf{u}\cdot\nabla)\,\mathbf{u} = (\nabla\times\mathbf{u})\times\mathbf{u} + \nabla\left[\frac{1}{2}\,|\mathbf{u}|\right], \tag{68}$$

we obtain

$$\frac{\partial \mathbf{u}}{\partial t} = -\eta\,\mathbf{k}\times\mathbf{u} - \nabla K - \frac{1}{\rho}\nabla p \tag{69}$$

where $\zeta = \mathbf{k}\cdot(\nabla\times\mathbf{u})$, $\eta = \zeta + f_o$ and the kinetic energy is defined as $K = \frac{1}{2}|\mathbf{u}|$.

Since the vector-invariant form of the evolution of momentum has no notion of a material derivative, it is a natural expression of the velocity tendency at a *fixed point in space*. The interesting and powerful aspect of (69) is that while $\mathbf{u}$ is defined at a point, the integral of $\mathbf{u}$ around a closed contour defines an area, a circulation and the area-mean vorticity. This relationship will be fully developed in Section 5.

The $\eta\,\mathbf{k}\times\mathbf{u}$ term will be referred to as the *nonlinear Coriolis force* because it contains both the linear tendency term $f_o\,\mathbf{k}\times\mathbf{u}$ and a portion of the nonlinear transport term in the form of $\zeta\,\mathbf{k}\times\mathbf{u}$.

When considering the momentum equation we are primarily interested in the velocity field that is needed for the evolution of the mass and tracer fields. Beyond the velocity itself, we are interested in three *derived* quantities: divergence, vorticity and kinetic energy. Two of these three derived quantities appear explicitly in (69). The appearance of vorticity and kinetic energy does not necessarily imply that the necessary controls are available to insure that these quantities remain well-behaved and bounded, but it is a step in the right direction.

In the context of climate modeling, it is difficult to find shortcomings in choosing the vector-invariant form of the momentum equation as the basis for a discrete model. This approach was successfully employed on hexagonal grids (Sadourny and Morel, 1969) and on latitude-longitude grids (Arakawa and Lamb, 1981) decades ago. The primary reason to not choose this form of the momentum equation is that another form of the momentum equation, such as the advective form or flux form, is a more natural choice for the application of interest.

4.4 The Vorticity-Diverenge Form

Since a great deal of emphasis has been placed on the importance of vorticity in the above discussion, it is reasonable to consider *exchanging* the prediction of the vector velocity for the prediction of the vorticity and divergence. As discussed above, the Helmoltz Decomposition guarantees that vorticity and divergence form a complete description of the vector velocity field, so prognosing ζ and δ is a theoretically-sound approach (e.g. Heikes and Randall (1995), Ringler et al (2000) and Thuburn (1997)). In addition, retaining ζ as a prognostic variable leads to a strong control over its evolution.

We generate the evolution equations for ζ and δ by taking $\nabla\times$ and $\nabla\cdot$ of the momentum equation, respectively. As long as we are working with the continuous equations, we can start with any form of the momentum equation and obtain the same resulting vorticity and divergence equation. Starting with the vector-invariant form of the momentum equation expressed in (69) and applying the $\mathbf{k}\cdot\nabla\times$ and $\nabla\cdot$ operators yields

$$\mathbf{k} \cdot \nabla \times \frac{\partial \mathbf{u}}{\partial t} = \frac{\partial \zeta}{\partial t} = \nabla \times \left[-\eta \mathbf{k} \times \mathbf{u} - \nabla K - \frac{1}{\rho} \nabla p \right], \tag{70}$$

and

$$\nabla \cdot \frac{\partial \mathbf{u}}{\partial t} = \frac{\partial \delta}{\partial t} = \nabla \cdot \left[-\eta \mathbf{k} \times \mathbf{u} - \nabla K - \frac{1}{\rho} \nabla p \right]. \tag{71}$$

Focusing on the vorticity equation, we can recover the Eulerian expression derived in (57) written as

$$\frac{\partial \eta}{\partial t} + \nabla \cdot (\eta \, \mathbf{u}) = -\nabla \times \left[\frac{\nabla p}{\rho} \right]. \tag{72}$$

The first important aspect to note in (72) is that $\mathbf{k} \cdot \nabla \times [-\eta \mathbf{k} \times \mathbf{u}] = \nabla \cdot (\eta \, \mathbf{u})$. The application of the curl operator to the nonlinear Coriolis force results in the divergence of the absolute vorticity flux. The second important aspect to note in (72) is that $\nabla \times \nabla K = 0$; the curl of the gradient is identically zero.

The divergence equation can be expressed as

$$\frac{\partial \delta}{\partial t} + \nabla \cdot \left(\eta \, \mathbf{u}^{\perp} \right) = -\nabla^2 K - \nabla \cdot \left[\frac{1}{\rho} \nabla p \right] \tag{73}$$

where $\mathbf{u}^{\perp} = \mathbf{k} \times \mathbf{u}$.

The primary advantage of using the vorticity-divergence form of the velocity evolution equation is the ability to retain (72) as a prognostic equation. In the presence of uniform density, the time-rate-of-chance of absolute vorticity is the divergence of the absolute vorticity flux. The absolute vorticity flux can be computed numerically using advanced transport algorithms that can guarantee that η will remain smooth at the grid-scale without the introduction of excessive dissipation.

The primary disadvantage of this formulation can be seen in (40) and (41). After each time step, two elliptic equations must be inverted in order to compute the velocity field that will be required to to compute the tendency terms in (72) and (73) on the next time step. For simple domains, such as the global atmosphere, inverting (40) and (41) is straightforward but relatively expensive in regards to computational effort. In more complicated domains, inverting (40) and (41) is analytically challenging and, at least to date, computationally prohibitive.

5 The process of discretization

In this section the continuous equations developed above will be *discretized* in order to obtain a numerical model for the evolution of momentum. The process of discretization truncates the infinite degrees of freedom that are present in the continuous system to a finite number of degrees of freedom in order to produce a computationally-tractable algebraic problem suitable for existing computer architectures. When the numerical methods are based on traditional finite-volume tech-

niques, such as those to be developed below, the spatial extent of the continuous system is decomposed into *cells* and the temporal extent of the continuous system is decomposed into *time steps*. The discussion here will be limited to the spatial discretization of the continuous system.

The possibilities for the specific form the discrete momentum equation can quickly become unwieldy. For example, the optimal way to decompose the sphere into cells is still very much a research topic. Even if we limit the scope to decompositions that attempt to produce quasi-uniform meshes the choices include, at a minimum, the cubed-sphere [check reference Nair chapter], Voronoi tessellations [check reference Ju chapter] and Delaunay triangulations [check reference Ju chapter]. Furthermore, once a mesh is chosen there are at least five different staggering arrangements of the prognostic variables: A-grid, B-grid, C-grid, D-grid, and E-grid (reference Thurburn chapter). In addition, we can choose one of the four viable flavors of $\mathbf{F} = m\mathbf{a}$ to discretize. So three meshes times five grid-staggerings times four momentum forms leads to sixty permutations. And this is before we even consider the specification of the numerical operators.

A "down-select" of the 60 permutations is required. Some of this down-select can be made based on the target application. Some of this down-select can be based on the wealth of experience that has been gained over the last forty years. And finally, some of this down-select can be made based on an intuition of what method(s) are likely to emerge as the preferred-alternative over the next decade. Furthermore, the selection method should not be made as an *a la carte* process; some choices of grid staggering are clearly inappropriate for certain choices in the form of the momentum equation. Rather, the process is similar to a *table d'hote* where choices are made with the prior knowledge of the other choices and the intention to produce the *best overall product* as opposed to the best single course. The courses in this chapter's *table d'hote* are discussed directly below.

5.1 Target application: Joint Climate-Weather Prediction

The traditional gap between atmosphere climate modeling and atmospheric weather prediction modeling is disappearing. Atmosphere climate models have been used to conduct global cloud resolving simulations (Tomita et al, 2005). Weather prediction models have been used to study regional climate change (Leung et al, 2004). While each model is finding application outside what has been its core mission, these uses are clearly "off-label applications" where, as expected, the quality of the results vary. The criteria driving the choices in model specification (i.e. the choice of mesh, grid staggering and form of momentum) have traditionally been very different in the climate and weather modeling communities. Climate applications have emphasized concepts related to mass, tracer and vorticity conservation, as well as long-time stability of numerical simulations. Weather applications have emphasized concepts related to local accuracy and simulation throughput. The driving need is for a *single* atmosphere model to excel at both climate applications and weather applications.

So the target application for this discussion is joint climate-weather simulations. As a result, the choices made below may differ from the choices made if the target application was solely climate simulation or solely weather prediction. And finally, these same choices will be applicable to a unified ocean model that is appropriate for both global ocean simulations and regional eddy-resolving simulations.

5.2 Grid staggering: C-grid Staggering

The choice of the grid staggering is very much constrained by the target application. Weather prediction models have often used a collocated staggering of variables in order to apply semi-Lagrangian methods to the advective form of the momentum equation (Ritchie et al, 1995). This is a computationally efficient method that is greatly appreciated in operational settings where simulation throughput is often a driving factor in model specification. Other grid staggerings, such as the B-grid (Zhang and Rancic, 2007) and C-grid staggering (Skamarock et al, 2008), have been used with success in both weather and climate models. The choice of the C-grid staggering, when paired with the other choices, will also allow for exact conservation of absolute vorticity[12]. And more importantly, the C-grid staggering will allow for the precise control of the evolution of vorticity in time through the use of advanced flux-limiting transport algorithms. In addition, the C-grid staggering excels in the simulation of divergent modes that dominate the cloud-resolving scales of motion (Randall, 1994). The principle difficulty with the C-grid staggering is that while the normal component of velocity is retained as a prognostic variable, the tangential component of velocity is needed to compute the nonlinear Coriolis force [check reference Thuburn chapter]. The robustness of numerical schemes built with a C-grid staggering is very much dependent on the method used for the reconstruction of the tangential velocity component.

5.3 Mesh: Locally-orthogonal meshes

One of the residual benefits of using the C-grid staggering is that it accommodates a wide class of meshes. The critical aspect of the C-grid staggering is that the edge that separates two cells is orthogonal to the line segment connecting the centers of the two associated cells [check reference Ju chapter]. The local orthogonality leads to compact numerical operators that are approximately 2nd-order accurate in space (Ringler et al, 2010). The local orthogonality, C-grid staggering and vector-

[12] While the target applications involve full 3D simulations of the atmosphere and ocean, the process of discretization is best elucidated in 2D. The 3D system is clearly more complicated and is not a simple extension of the 2D system. Still, the concept of vorticity dynamics and conservation of (potential) vorticity are equally important in the full 3D system

invariant form of momentum will lead to a strong connection between acceleration and vorticity transport.

5.4 Form of momentum equation: The Vector-Invariant Form

The use of the vector-invariant form of the momentum equation has a long and successful track record in climate modeling dating back to at least (Arakawa and Lamb, 1981). Weather applications have tended to use other forms, such as the flux form (e.g. Weather and Research Forecast (WRF) model (Skamarock et al, 2008) in order to conserve momentum and to obtain higher formal accuracy or the advective form (e.g. European Center for Medium-Range Weather Forecasts (ECMWF) model (Ritchie et al, 1995) in order to employ semi-Lagrangian methods.

The comparison of the vector-invariant form to the flux form offers an important insight into conservation. Given all of the choices made above (i.e. climate-weather applications, C-grid staggering, and locally-orthogonal meshes), either the vector-invariant form or the flux form is a viable choice. If one chooses the flux form of the momentum equation, then the prognostic variable, $\rho \mathbf{u}$, will be conserved in the numerical model. As derived below, if one chooses the vector-invariant form of the momentum equation, then absolute vorticity will be conserved in the numerical model. The choice between the vector-invariant form or the flux form of momentum comes down to the relative importance of conserving absolute vorticity or conserving momentum in the target application. The choice here is to value the former more than the latter.

6 Building a Discrete Model

This section will develop the numerical model that uses a C-grid staggering of the vector-invariant form of the momentum equation discretized on a locally-orthogonal mesh. The analysis will focus on the relationship between the time-tendency of the velocity field and the absolute vorticity flux.

6.1 Defining the Mesh and Location of Variables

For this discussion we will assume that the domain is decomposed into a set of squares as shown in Figure 7. As seen in Figure 7, the scalar function, Φ, is defined at the center of each cell. The component of velocity in the direction normal to each edge will be integrated in time with a prognostic equation. Vorticity points are defined at the corners of the scalar function cells and will be associated with

the mesh denoted by the dashed lines. The assumption is that the mesh continues indefinitely in all horizontal directions.

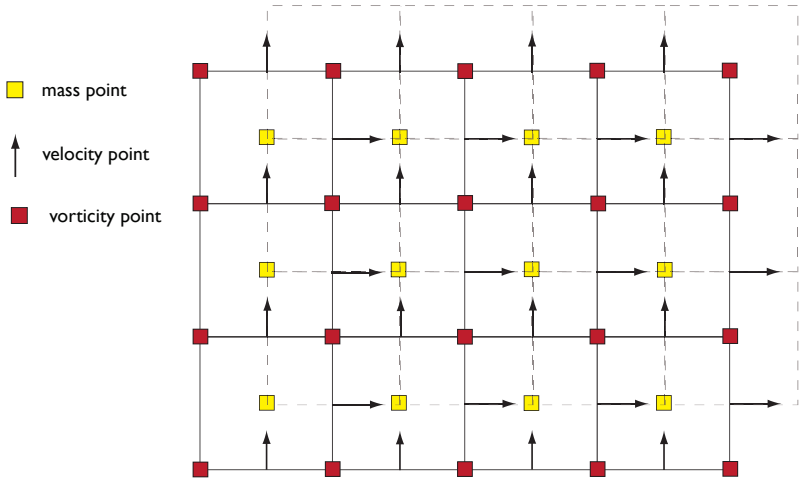

Fig. 7: The mesh used in the construction of the discrete system.

The choice of squares as the cell shape is based on several reasons. A mesh composed of squares is clearly locally-orthogonal, so it meets the requirement listed in Section 5. A mesh composed of squares is also the most accessible mesh; the analysis presented here can be easily replicated in development environments such as MATLAB.

While the derivation will be completed for a mesh composed of squares, conformally-mapped cubed-sphere meshes, Voronoi tessellations and Delaunay triangulations are all accommodated in the analysis[13], i.e. the results found for the mesh composed of squares will be applicable to these more practical meshes. In an effort to point the way toward extensions to meshes that are used to discretize the surface of the sphere, an indexing nomenclature will be chosen that is appropriate for any unstructured mesh.

[13] Cubed-sphere grids produced by projections that result in a more uniform distribution of nodes at the at expense of orthogonality (e.g. gnomonic-projected cubed-sphere meshes) are not accommodated in this analysis

6.2 Continuous Prognostic Equation

We discretize the vector-invariant form of the momentum equation as

$$\frac{\partial \mathbf{u}}{\partial t} + \eta\, \mathbf{k} \times \mathbf{u} = -\nabla \Phi \tag{74}$$

where $-\nabla\Phi = -\nabla\left(\frac{p}{\rho_o} + K\right)$ represents the gradient terms on the RHS of (69). In the full 3D system, ρ will vary in space and, as a result, the RHS can not be written as the gradient of a potential. Here, the analysis assumes that the density is a constant ρ_o in order to demonstrate that the largest contribution to the RHS of (69) (i.e. the ρ_o contribution) does not project onto the vorticity dynamics of the system. The system can be closed by the addition of an equation describing the evolution of fluid pressure, p. For reasons discussed in the Section 1, we will limit the analysis to the evolution of velocity.

The $\mathbf{k} \times \mathbf{u}$ operation acts to rotate the vector velocity by 90 degrees in the counter clockwise direction. If we define $\mathbf{u}^\perp = \mathbf{k} \times \mathbf{u}$ as in (73) then (74) is expressed as

$$\frac{\partial \mathbf{u}}{\partial t} + \eta\, \mathbf{u}^\perp = -\nabla \Phi. \tag{75}$$

6.3 Discrete Prognostic Equation

At each cell edge the unit normal vector $\mathbf{e}_N$ is defined to point toward the right or toward the top as appropriate.[14] In addition, the tangential unit vector is defined as $\mathbf{e}_T = \mathbf{k} \times \mathbf{e}_N$. The discrete version of (75) is generated by taking $\mathbf{e}_N \cdot$ (75) at each edge to yield

$$\frac{\partial N_k}{\partial t} - \hat{\eta}_k \hat{T}_k = -\left(\mathbf{e}_N \cdot \nabla \Phi\right)_k \tag{76}$$

where, as shown in Figure 8, $N_k = \mathbf{e}_N \cdot \mathbf{u}$ represents the component of $\mathbf{u}$ in the normal direction and $\hat{T}_k = -\mathbf{e}_N \cdot \mathbf{u}^\perp$ represents the component of $\mathbf{u}$ in the tangential direction. All variables with hats, $\hat{(\cdot)}$, require further specification.

The first example of the simplicity afforded by the assumption of a locally-orthogonal mesh is found on the RHS of (76). The RHS of (76) requires the determination of the component of $\nabla\Phi$ in the $\mathbf{e}_N$ direction. Since $\mathbf{e}_N$ is parallel to the vector connecting the Φ points on either side of the edge, the specification of the $\left(\mathbf{e}_N \cdot \nabla\Phi\right)_k$ can be approximated (with 2nd-order accuracy) at velocity point k_1 as simply $\left[\Phi_{i_4} - \Phi_{i_1}\right]/dc_{k_1}$ (See Figure 8). Using this representation of the gradient forcing, (76) at velocity point k_1 is rewritten as

[14] The choice of the direction of the local normal vector is entirely arbitrary. The choice made here is for the convenience of presentation.

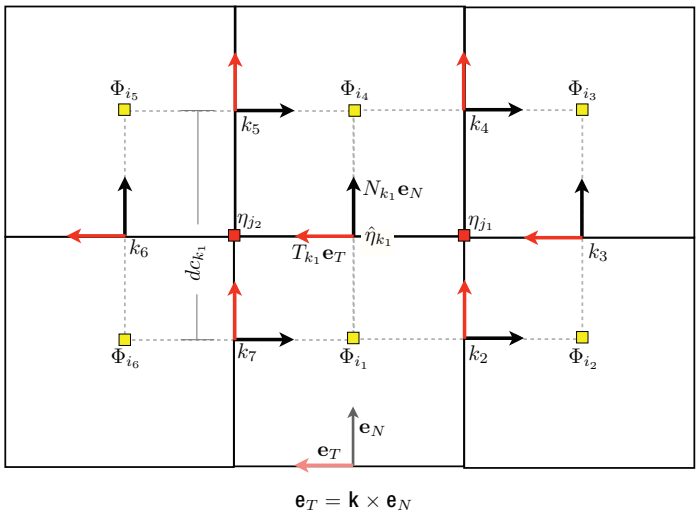

Fig. 8: The detailed description of the velocity and vorticity mesh.

$$\frac{\partial N_{k_1}}{\partial t} = \hat{\eta}_{k_1} \hat{T}_{k_1} - [\Phi_{i_4} - \Phi_{i_1}]/dc_{k_1} \tag{77}$$

where dc_{k_1} is the distance between Φ_{i_4} and Φ_{i_1}. While the various ways to specify $\hat{\eta}_{k_1}$ is given in Section 7, at this point $\hat{\eta}_{k_1}$ can be constrained as

$$\hat{\eta}_{k_1} = f(\eta_{j_1}, \eta_{j_2}). \tag{78}$$

The absolute vorticity used to compute the nonlinear Coriolis force, $\hat{\eta}\hat{T}$, at velocity points is only a function of the vorticities defined at the end of the edge.[15] In order to complete the specification of (77) a definition for $\hat{T}_{k_1}$ is required. The algorithm for computing $\hat{T}_{k_1}$ is also given in Section 7.

6.4 Discrete Derived Equation

The importance of discrete derived equations is frequently overlooked. Attention is more often focused on the analysis of the discrete prognostic equations since

[15] Other approaches to specifying $\hat{\eta}$ are possible and often preferable. See (Sadourny, 1975) and (Ringler et al, 2010) for a more in depth discussion of the possible alternatives.

these are the variables that are explicitly tracked in time. In reality, an analysis of the discrete derived equations generally provides important insights into the chosen numerical method. The purpose of this section is to demonstrate that the discrete system can mimic the continuous system in terms of the vorticity dynamics. The analysis carried out in Section 3.4.1 and Section 3.4.2 is repeated here, but in the setting of a discrete system. The primary property of the continuous system that the discrete system needs to mimic is

$$\frac{d}{dt}\Gamma^a_{c(t)} = \frac{d}{dt}\left[\int\limits_{S(t)} \eta \, dS\right] = \int\limits_{S} \left[\frac{\partial \eta}{\partial t} + \nabla \cdot (\eta \, \mathbf{u})\right] dS = 0. \tag{79}$$

The absolute circulation following a contour $c(t)$ is conserved when the fluid density is constant (as is assumed here) and when no frictional forces are present. The challenge is to demonstrate that absolute circulation is conserved following a contour $c(t)$ *even when the discrete system does not directly prognose circulation or vorticity.* Stated another way, the goal is to demonstrate that the evolution of the discrete velocity field, N_k, is consistent with the kinematic constraints imposed by (79). Since the velocity evolution equation is written in an Eulerian reference frame, the analysis is most direct when the focus is on the third part of (79). The integration of dS can span a single cell or a collection of cells that are contained in a single loop.

The analysis begins by taking the discrete curl of the velocity tendency equation around the j_1 vorticity cell shown in Figure 8. The discrete circulation operator is shown in Figure 9. As seen in Figure 9 the discrete curl has four terms, one for each edge of a vorticity cell. Using the labels shown in Figure 9, the curl operator at vorticity point j_1 can be expressed as

$$\frac{1}{A}\oint\limits_{c} \mathbf{u} \cdot \mathbf{dr} \approx \frac{1}{A_{j_1}} \sum_{m=1}^{4} N_{k_m} \, \mathbf{e}_N \cdot \mathbf{dr}_{k_m} \tag{80}$$

where A_{j_1} is the area of the vorticity cell j_1. The dot product $\mathbf{e}_N \cdot \mathbf{dr}_{k_m}$ accounts for whether or not $N_{k_m}\,\mathbf{e}_N$ points in the same or the opposite direction as $\mathbf{dr}_{k_m}$. In addition, $|\mathbf{dr}_{k_m}| = dc_{k_m}$ to account for the distance of each segment of the loop around vorticity cell j_1.

A discrete equation for the evolution of absolute vorticity is constructed by applying the curl operator to each term in (77). In order to provide a clear representation of the curl operations, we will focus on vorticity point j_1. Beginning with the discrete curl of the time tendency of N_k, we find

$$\frac{1}{A}\oint\limits_{c} \frac{\partial \mathbf{u}}{\partial t} \cdot \mathbf{dr} \approx \frac{1}{A_{j_1}} \sum_{m=1}^{4} \frac{\partial N_{k_m}}{\partial t} \, \mathbf{e}_N \cdot \mathbf{dr}_{k_m} = \frac{\partial \zeta_{j_1}}{\partial t} = \frac{\partial \eta_{j_1}}{\partial t} \tag{81}$$

where the curl operator has been moved inside the time derivative and we have used the fact that $\frac{\partial f_o}{\partial t} = 0$. Now moving to the gradient term on the RHS of (77) we find

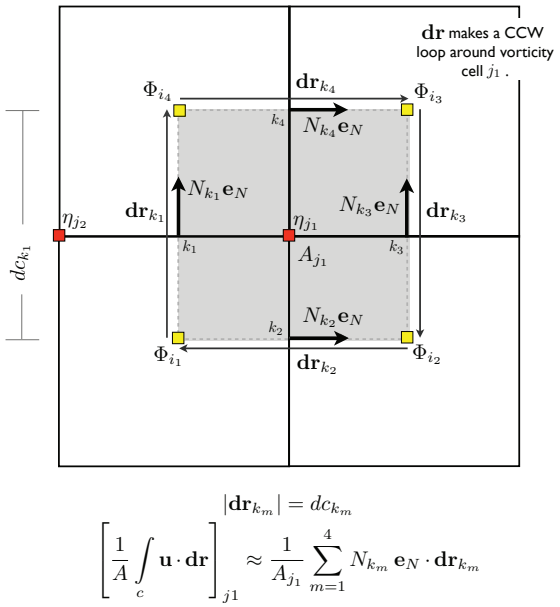

Fig. 9: A graphical description of the discrete curl operator.

$$-\frac{1}{A}\oint_c \nabla\Phi\cdot\mathbf{dr} \approx \frac{1}{A_j}\left[\frac{(\Phi_2-\Phi_1)}{dc_{k_2}}dc_{k_2}+\frac{(\Phi_3-\Phi_2)}{dc_{k_3}}dc_{k_3}-\frac{(\Phi_3-\Phi_4)}{dc_{k_4}}dc_{k_4}-\frac{(\Phi_4-\Phi_1)}{dc_{k_1}}dc_{k_1}\right] \tag{82}$$

where the distance used in the gradient calculation and the distance used in the curl operator cancel on each term. After removing these offsetting terms we find

$$\frac{1}{A}\oint_c \nabla\Phi\cdot\mathbf{dr} \approx \frac{1}{A_j}\left[(\Phi_2-\Phi_1)+(\Phi_3-\Phi_2)+(\Phi_4-\Phi_3)+(\Phi_1-\Phi_4)\right]. \tag{83}$$

Just as in the continuous system, the curl of the gradient is identically zero. This property in the discrete system insures that forces in the velocity tendency equation of the form $\nabla\Phi$, where Φ is any scalar field defined at mass points, do not generate spurious vorticity.

Moving to the final term, the nonlinear Coriolis force, we find

$$\frac{1}{A}\oint_c \eta\,\mathbf{u}^{\perp}\cdot\mathbf{dr} \approx -\frac{1}{A_{j_1}}\sum_{m=1}^{4}\hat{\eta}_{k_m}\hat{T}_{k_m}\,\mathbf{e}_{N_{km}}\cdot\mathbf{dr}_{k_m}. \tag{84}$$

Expanding the summation yields

$$-\frac{1}{A_j}\sum_{m=1}^{4}\left(\hat{\eta}\hat{T}\,\mathbf{e}_N\right)_{k_m}\cdot\mathbf{dr}_{k_m}=-\frac{1}{A_j}\left[+\left(\hat{\eta}\hat{T}dc\right)_{k_1}-\left(\hat{\eta}\hat{T}dc\right)_{k_2}-\left(\hat{\eta}\hat{T}dc\right)_{k_3}+\left(\hat{\eta}\hat{T}dc\right)_{k_4}\right]. \tag{85}$$

Combining all of the curl operators to produce a discrete equation for the evolution of absolute vorticity yields

$$\frac{\partial\eta_{j_1}}{\partial t}+\frac{1}{A_{j_1}}\left[+\left(\hat{\eta}\hat{T}dc\right)_{k_1}-\left(\hat{\eta}\hat{T}dc\right)_{k_2}-\left(\hat{\eta}\hat{T}dc\right)_{k_3}+\left(\hat{\eta}\hat{T}dc\right)_{k_4}\right]=0. \tag{86}$$

Comparing (86) to its continuous counterpart in (57), we see that the discrete vorticity evolution equation is an analog to the continuous system when

$$\nabla\cdot(\eta\,\mathbf{u})\approx\frac{1}{A_{j_1}}\left[+\left(\hat{\eta}\hat{T}dc\right)_{k_1}-\left(\hat{\eta}\hat{T}dc\right)_{k_2}-\left(\hat{\eta}\hat{T}dc\right)_{k_3}+\left(\hat{\eta}\hat{T}dc\right)_{k_4}\right]. \tag{87}$$

The RHS of (87) is an approximation to the weak form of the divergence operator.[16] It is critical to note that in this discrete system *vorticity is transported by the reconstructed, tangential velocity field*. It is useful to recast (86) as an expression for the circulation within cell j_1 by moving the area into the time derivative as

$$A_{j_1}\frac{\partial\eta_{j_1}}{\partial t}=\frac{\partial\Gamma^a_{j_1}}{\partial t}=-\left[+\left(\hat{\eta}\hat{T}dc\right)_{k_1}-\left(\hat{\eta}\hat{T}dc\right)_{k_2}-\left(\hat{\eta}\hat{T}dc\right)_{k_3}+\left(\hat{\eta}\hat{T}dc\right)_{k_4}\right]. \tag{88}$$

$\Gamma^a_{j_1}$ represents the absolute circulation around the dual cell j_1. This result can be generalized to an arbitrary contour by progressively adding cells. Equation (88) represents a contour containing the j_1 vorticity cell. The discrete equation governing the evolution of circulation for the j_2 vorticity cell can be expressed as

$$\frac{\partial\Gamma_{j_2}}{\partial t}=-\left[-\left(\hat{\eta}\hat{T}dc\right)_{k_1}+\left(\hat{\eta}\hat{T}dc\right)_{k_5}+\left(\hat{\eta}\hat{T}dc\right)_{k_6}-\left(\hat{\eta}\hat{T}dc\right)_{k_7}\right]. \tag{89}$$

The edge shared by vorticity cells j_1 and j_2 is edge k_1. The term $\left(\hat{\eta}\hat{T}dc\right)_{k_1}$ appears in both (88) and (89), but with opposite signs. The evolution of absolute circulation formed by the contour containing vorticity cell j_1 and j_2 is thus

$$\frac{\partial(\Gamma_{j_1}+\Gamma_{j_2})}{\partial t}=-\left[-\left(\hat{\eta}\hat{T}dc\right)_{k_2}-\left(\hat{\eta}\hat{T}dc\right)_{k_3}+\left(\hat{\eta}\hat{T}dc\right)_{k_4}+\left(\hat{\eta}\hat{T}dc\right)_{k_5}+\left(\hat{\eta}\hat{T}dc\right)_{k_6}-\left(\hat{\eta}\hat{T}dc\right)_{k_7}\right] \tag{90}$$

where the shared edge between vorticity cells j_1 and j_2 cancels. The edges that remain all lie on the boundary of the contour and account for the transport of circulation across the boundary of the region. The mean absolute vorticity within the contour can always be determined by dividing the absolute circulation by the area

[16] The approximation is 2nd-order accurate assuming suitable choices for $\hat{\eta}$ and $\hat{T}$.

enclosed in the contour. This analysis is sufficient to state that the discrete system conserves absolute circulation exactly. By extension, the discrete system conserves the area-mean absolute vorticity exactly. Both of these conservation statements mimic the findings in the continuous system. What is somewhat surprising is that these conservation statements have been proven *without even having to specify* $\hat{\eta}$ *or* $\hat{T}$. In that, the conservation statements hold for any $\hat{\eta}$ and any $\hat{T}$. The two essential ingredients required for these conservation statements to hold in the discrete system are the use of the vector-invariant form of the momentum equation and the discrete analog of the $\nabla \times \nabla \Phi \equiv 0$ identity.

The final and most important conclusion of this section is the following: The time tendency of velocity due to the nonlinear Coriolis force $\left(\hat{\eta}\hat{T}\right)$ **is** the per-unit-length absolute vorticity transport in the direction normal to $\mathbf{e}_N$. This is key to providing a direct handle on the vorticity dynamics of the discrete system via the discrete momentum equation.

7 Constraining the Evolution of Velocity through the Transport of Absolute Vorticity

In the preceding section we were able to accomplish three goals. First, we were able to exhibit that absolute circulation is conserved for any closed loop in the discrete system. Second, the conservation statements related to circulation and vorticity hold exactly in the discrete system, even though neither are retained as prognostic variables. And finally, these conservation statements hold without having to specify the form of the reconstructed tangential velocity or the value of absolute vorticity used to compute the velocity tendency due to the nonlinear Coriolis force. Given this last statement, it should be clear that conservation alone is insufficient in specifying an adequate numerical model. The general framework allows us to specify $\hat{\eta}$ and $\hat{T}$ to meet other constraints that we deem important. The following discussion is meant to demonstrate the flexibility, or lack thereof, in the choice of $\hat{\eta}$ and $\hat{T}$. It turns out that there is some flexibility in the choice of the former and essentially no flexibility in the choice of the latter. As above, constant density and non-divergent flow are assumed.

7.1 Considerations when specifying $\hat{\eta}$

The specification of $\hat{\eta}$ should be made with two concerns in mind. The first is that since the nonlinear Coriolis force $\eta\,\mathbf{k}\times\mathbf{u}$ is alway orthogonal to $\mathbf{u}$, the nonlinear Coriolis force neither produces nor destroys kinetic energy, i.e. $\mathbf{u}\cdot(\eta\,\mathbf{k}\times\mathbf{u}) = 0$. This is essentially a concern related to the energetics of the discrete system. The second concern is how the specification of $\hat{\eta}$ will influence the structure of the evolving vorticity field. For example, we would like to make some guarantees on

the long-time smoothness of the discrete vorticity field. This is essentially a concern related to the vorticity dynamics of the discrete system. The goal, in my view, should be the rigorous guarantee of both of these concerns. In that, the guarantee that the choice of $\hat{\eta}$ neither produces or destroys kinetic energy *and* that this same choice in $\hat{\eta}$ promotes long-term smoothness in the vorticity field. Given the analysis and the anecdotal evidence presented in (Ringler et al, 2010), this goal might be possible.

For the discussion presented here, the focus will be on choosing $\hat{\eta}$ such that the evolution of absolute vorticity is monotone in time.[17] In the context of transport, monotonicity implies that the vorticity field at some time t can be determined as a *convex interpolation* of the vorticity field at some previous time (Godunov, 1959). Since the interpolation process is *convex*, vorticity values at some previous time are given weights between zero and one. Thus monotonicity implies that the solution of vorticity at any time t is bounded from above and below by the vorticity at any previous time. While it is true that only in the special case of non-divergent flow should we expect absolute vorticity to evolve monotonically in time, extensions of this idea to potential vorticity holds for general 3D flows. If we assume an arbitrary velocity field that is non-divergent, then the continuous vorticity equation (58) reduces to

$$\frac{\partial \eta}{\partial t} + \nabla \cdot (\eta \, \mathbf{u}) = \frac{\partial \eta}{\partial t} + \mathbf{u} \cdot \nabla \eta = \frac{D\eta}{Dt} = 0, \tag{91}$$

which states that the absolute vorticity attributed to a particle (e.g. Figure 1) is invariant in time. Since we are not in a Lagrangian reference frame where tracking particles is an option, the discrete model will have to attempt to mimic (91) in an Eulerian setting. When a property is conserved along particle trajectories it means that the quantity itself (e.g. η) and all moments of that quantity (e.g. η^n where n is any integer) are also conserved along particle trajectories. With only one degree of freedom in the discrete system (i.e. $\hat{\eta}$), we are woefully ill-equipped to mimic the richness contained in the continuous system and, therefore, must make some tough choices regarding how to specify $\hat{\eta}$. The goal here is not to determine an optimal specification of $\hat{\eta}$ but rather to demonstrate that we can *guarantee* a monotone evolution of vorticity even when the only prognostic variable is the normal component of velocity at cell edges.

Assuming that the discrete velocity field is non-divergent, guaranteeing a monotone evolution of the discrete absolute vorticity field is straightforward. Focusing on edge (k_1), we specify $\hat{\eta}_{k_1}$ as

$$if \ \hat{T}_{k_1} \geq 0, \ \hat{\eta}_{k_1} = \eta_{j_1} \tag{92}$$

$$if \ \hat{T}_{k_1} < 0, \ \hat{\eta}_{k_1} = \eta_{j_2} \tag{93}$$

[17] Discussing the evolution of potential vorticity, as opposed to absolute vorticity, would be more relevant here. But for the reasons discussed in the Introduction, we will limit the scope to the evolution of absolute vorticity. Only in the special case of non-divergent flow is the evolution of absolute vorticity monotone. In addition, the topic of transport (monotone or otherwise) warrants an entire chapter to itself.

in that we always choose the value of $\hat{\eta}$ by picking the vorticity value *upstream of* $\hat{T}$. While this is essential the low-order, monotone solution used in (Zalesak, 1979), it immediately generalizes to higher-order. Without loss of generality, assume that $\hat{T} \geq 0$ at some instant in time, then the evolution equation of N_{k_1} is written as

$$\frac{\partial N_{k_1}}{\partial t} = \eta_{j_1} \hat{T}_{k_1} - [\Phi_{i_4} - \Phi_{i_1}] / dc_{k_1}. \tag{94}$$

If $\hat{\eta}$ is chosen based on the approach in (92), then the absolute vorticity associated with the evolving N_k velocity field will be monotone. To be clear, the donor cell approach results in excessive diffusion and this discussion is in no way meant to advocate for the use of (92); it is employed here for demonstration purposes only. In practice, we can apply state-of-the-art transport algorithms for the computation of the absolute vorticity flux, $\hat{\eta}\hat{T}$, and use that flux as the nonlinear Coriolis force in the velocity tendency equation.

7.2 Considerations when specifying $\hat{T}$

It turns out that there is essentially no flexibility in the choice of $\hat{T}$. The mesh used here is essentially identical to that used in (Arakawa and Lamb, 1981). In that work, the reconstructed velocity is specified as

$$\hat{T}_{k_1} = -\frac{1}{4}\left(N_{k_7} + N_{k_2} + N_{k_4} + N_{k_5}\right). \tag{95}$$

See Figure 8. The reasoning behind this choice is not particularly clear in the (Arakawa and Lamb, 1981) manuscript. Based on the more recent analysis conducted on general unstructured meshes with C-grid staggerings in (Thuburn et al, 2009) and (Ringler et al, 2010), it is clear that the critically important aspect of the reconstructed $\hat{T}$ field is that the $\left[\nabla \cdot \left(\hat{T}\,\mathbf{e}_T\right)\right]_j$ be an interpolation of the neighboring $\left[\nabla \cdot (N\,\mathbf{e}_N)\right]_i$ values; the divergence computed at vorticity points based on $\hat{T}_k$ *must* be an interpolation of the divergence computed at mass points based on N_k.

The importance and significance of this requirement can be clearly seen in the following example. Suppose the continuous system is characterized with an initial condition of uniform absolute vorticity field being transported by a non-divergent flow. From (58) we see that the solution for all time is simply $\frac{\partial \eta}{\partial t} = 0$. Also suppose that the discrete velocity field N_k is chosen such that it produces a uniform absolute vorticity field and is also non-divergent. The discrete system from (86) can be expressed as

$$\frac{\partial \eta_{j_1}}{\partial t} + \frac{\eta_o}{A_{j_1}}\left[\left(\hat{T}dc\right)_{k_1} + \left(\hat{T}dc\right)_{k_2} - \left(\hat{T}dc\right)_{k_3} - \left(\hat{T}dc\right)_{k_4}\right] = 0 \tag{96}$$

The only way to reproduce the solution of $\frac{\partial \eta}{\partial t} = 0$ for all time is to require that

$$\left[\left(\hat{T}dc\right)_{k_1} + \left(\hat{T}dc\right)_{k_2} - \left(\hat{T}dc\right)_{k_3} - \left(\hat{T}dc\right)_{k_4}\right] = 0. \tag{97}$$

Equation (97) requires that the divergence of the reconstructed, tangential velocity at vorticity points is also zero. If one can build a general algorithm for the reconstruction of $\hat{T}$ that produces $\left[\nabla\cdot\left(\hat{T}\,\mathbf{e}_T\right)\right]_j = 0$ when $\left[\nabla\cdot\left(N\,\mathbf{e}_N\right)\right]_i = 0$, then we have sufficient proof that the divergence computed at vorticity points will be a convex interpolation of the divergence computed at mass points. Unfortunately, the failure of some C-grid staggered model to enforce this essential feature in the reconstruction of the tangential velocity has lead to (sometime severes) limitations in the robustness of the numerical model and the quality of the numerical solutions.

8 Final Thoughts

This analysis provided an end-to-end discussion of one aspect in the construction of a dynamical core, namely the derivation and approximation of the equations related to the evolution of momentum. As much as possible, the analysis is developed with the aid of the Reynolds Transport Theorem. In addition to providing a rigorous means to recasting conservation statements made in the Lagrangian reference frame to statements applicable to the Eulerian reference frame, the Reynolds Transport Theorem produces evolution equations cast in a weak, integral form that fit naturally into traditional finite-volume approaches.

The analysis lingered and continually revisited the relationship between the evolution of velocity and vorticity dynamics. The reason for such a strong emphasis on this relationship is that while the evolution of momentum has to be faithful to $\mathbf{F} = m\,\mathbf{a}$, it also has to respect the kinematic constraints implied by conservation statements related to vorticity and circulation. First, the relationship has to be understood in the continuous setting, then the relationship has to be accommodated in the development of the discrete system of equations.

The system of equations that one chooses as the starting point for constructing a discrete model is a critical moment in the construction of a dynamical core. This choice will have a profound impact on the quality of the simulations. Understanding the anticipated use of the numerical model is a prerequisite to making sound, defensible choices for the components of a dynamical core. For this reason, an entire section related to the ”process of discretization” is included. While the actual choices made in that section are highly biased, the purpose of the section is to hopefully motivate the extreme importance of choosing numerical methods based on a target application.

Acknowledgements This work was supported by the DOE Office of Science’s Climate Change Prediction Program DOE 07SCPF152. I would like to thank Professor Sidney Leibovich for providing a thorough training in the foundation of fluid dynamics. In addition, I would like to thank Professor David Randall for his mentoring and invaluable insights into the construction of ro-

bust numerical algorithms. The chapter benefited greatly from a critical reviews provided by John Dukowicz, an anonymous reviewer, and the editors.

References

Arakawa A (1997) Computational design for long-term numerical integration of the equations of fluid motion: Two-dimensional incompressible. Journal of Computational Physics 135,:103–114

Arakawa A, Lamb V (1981) A potential enstrophy and energy conserving scheme for the shallow water equations. Monthly Weather Review pp 18–36

Batchelor GK (1967) Introduction to fluid dynamics. Cambridge Press

Bleck R, Smith L (1990) A wind-driven isopycnic coordinate model of the north and equatorial atlantic ocean. 1. model .... J Geophys Res 95(C3):32733285

Dixon M, Ringler T (2010, submitted) Conservative properties of a variational free-lagrange method for shallow water. Discrete and Continuous Dynamical Systems

Godunov SK (1959) A difference method for numerical calculation of discontinuous solutions of the equations of hydrodynamics. Mat Sb 47(89):3:271–306

Haertel P, Roekel LV, Jensen T (2009) Constructing an idealized model of the north atlantic ocean using slippery sacks. Ocean Modelling 27:143–159

Heikes R, Randall D (1995) Numerical integration of the shallow-water equations on a twisted icosahedral grid. part i: Basic design and results of tests. Monthly Weather Review 123:1862–1880

Hirt C, Amsden A, Cook J (1997) An arbitrary lagrangian-eulerian computing method for all flow speeds. Journal of Computational Physics 135(2):203–216

Konor C, Arakawa A (1997) Design of an atmospheric model based on a generalized vertical coordinate. Monthly Weather Review 125:1649–1673

Leung LR, Qian Y, Bian X, Washington WM, Han J, Roads JO (2004) Mid-century ensemble regional climate change scenarios for the western united states. Climatic Change 62(1-3):75–113

Randall D (1994) Geostrophic adjustment and the finite-difference shallow-water equations. Monthly Weather Review 122(6):1371–1377

Ringler, Thurburn, Klemp, Skamarock (2010) Numerical treatment of energy and potential vorticity on arbitrarily structured c-grids. Journal of Computational Physics 229:30653090

Ringler T, Heikes R, Randall D (2000) Modeling the atmospheric general circulation using a spherical geodesic grid: A new class of dynamical cores. Monthly Weather Review 128(7):2471–2490

Ritchie H, Temperton C, Simmons A, Hortal M, Davies T, Dent D, Hamrud M (1995) Implementation of the semi-lagrangian method in a high-resolution version of the ecmwf forecast model. Monthly Weather Review 123(2):489–514

Sadourny R (1975) The dynamics of finite-difference models of the shallow-water equations. Journal of the Atmospheric Sciences 32(4):680–689

Sadourny R, Morel P (1969) A finite-difference approximation of the primitive equations for a hexagonal grid on a plane. Monthly Weather Review 97(6):439–445

Skamarock W, Klemp J, Dudhia J, Gill D, Barker D, Duda M, Huang X, Wang W, Powers J (2008) A description of the advanced research wrf version 3. NCAR TECHNICAL NOTE

Staniforth A, Cote J (1991) Semi-lagrangian integration schemes for atmospheric models—a review. Monthly Weather Review 119(9):2206–2223

Thuburn J (1997) A pv-based shallow-water model on a hexagonal–icosahedral grid. Monthly Weather Review 125(9):2328–2347

Thuburn J, Ringler T, Skamarock W, Klemp J (2009) Numerical representation of geostrophic modes on arbitrarily structured c-grids. Journal of Computational Physics 228(22):8321–8335

Tomita H, Miura H, Iga S, Nasuno T, Satoh M (2005) A global cloud-resolving simulation: Preliminary results from an aqua planet experiment. Geophys Res Lett 32(8):L08,805

White F (2008) Fluid mechanics. McGraw-Hill Higher Education

Zalesak S (1979) Fully multidimensional flux-corrected transport algorithms for fluids. Journal of Computational Physics 31(3):335–362

Zhang H, Rancic M (2007) A global eta model on quasi-uniform grids. Q J R Meteorol Soc 133(623):517–528